

TABLE 1. Globular Clusters Used for Calibration

Cluster	V_{HB}	$E(B - V)$	[Fe/H]	W' (Å)	m.e. (Å)
NGC 104	14.06	0.04	-0.71	4.79	0.03
NGC 3201	14.80	0.21	-1.56	3.59	0.04
NGC 5139	14.54	0.11
NGC 6121	13.35	0.40	-1.33	4.13	0.03
NGC 6397	12.90	0.18	-1.91	2.27	0.03

Notes to Table 1.

Sources for photometry and star names. NGC 104 (47 Tucanae): Cudworth (1994), CF names from Chun & Freeman 1978, L names from Lee 1977b, W names from Wildey 1961, LE from Llyod Evans (1974). NGC 3201: Côte (private communication), L names from Lee 1977c. NGC 5139 (ω Cen): Woolley 1966. Photometry discussed in text. NGC 6121 (M4): Cudworth & Rees 1990 (photometry), Lee 1977a (names). NGC 6397: Woolley et al. (1961) and Cannon (1974).

TABLE 2. Photometry, EQW values, and Radial Velocities for Standard Clusters

Star	$V - V_{HB}$	$(B - V)_0$	$\log_{10}(\text{Int})$ (e ⁻)	v_r (km s ⁻¹)	$\sigma(v_r)$ (km s ⁻¹)	W(Ca) (Å)	$\sigma(\text{W}(\text{Ca}))$ (Å)	N	Notes
NGC 104 (47 Tucanae)									
CF4145/W206	-2.24	1.58	4.532	-11.2	0.1	6.14	0.06	2	
CF3116/L3512	-2.23	1.58	4.633	-17.4	1.1	6.16	0.02	2	1
CF3350/L1603	-2.23	1.58	4.461	-15.8	1.7	5.97	0.10	2	
CF4267/L2705	-2.23	1.59	4.773	-21.0	0.5	5.71	0.13	2	1,2,3
CF3659/L5622	-2.20	1.66	4.635	-21.0	0.4	5.77	0.03	2	3,4
CF4615/L7701	-2.18	1.54	4.689	-23.7	0.6	6.31	0.07	2	1
CF4331/W115	-2.12	1.52	4.445	-17.2	0.1	6.03	0.01	2	
CF4608/L7726	-2.02	1.46	4.792	-25.9	0.4	6.11	0.03	2	3,4,5
CF3133/L3708	-1.98	1.46	4.451	-32.8	0.9	6.02	0.13	2	
CF3658/L5623	-1.85	1.39	4.274	-27.9	0.1	5.96	0.03	2	
CF3454/L8636	-1.83	1.36	4.153	-14.4	1.0	5.86	0.04	2	3
CF3319/L1605	-1.72	1.45	4.162	-9.6	2.3	6.18	0.13	2	6
CF4551/L6764	-1.70	1.34	4.226	-16.9	1.0	6.11	0.09	2	
CF4472/L5739	-1.63	1.33	4.207	-31.9	0.2	5.93	0.13	2	
CF3886/L5627	-1.60	1.24	4.233	-9.3	0.1	5.66	0.06	2	7
CF3579/L6527	-1.59	1.32	4.004	-26.2	0.1	5.97	0.01	2	
CF3208/L2605	-1.56	1.23	4.135	-19.1	0.9	5.68	0.14	2	3,7
CF4015/W221	-1.49	1.28	4.081	-4.7	2.7	5.52	0.28	2	3
CF3101/L3622	-1.37	1.18	3.752	-13.5	0.7	5.64	0.05	2	7
CF4399/W92	-1.25	1.22	3.958	-26.3	4.2	5.38	0.00	2	
CF4525/L6728	-1.24	1.24	4.055	-16.1	0.9	5.83	0.01	2	3
CF3223/L2603	-1.16	1.25	4.040	-20.8	0.1	5.63	0.04	2	
CF4326/W125	-1.00	1.18	3.875	-12.8	0.6	5.42	0.04	2	
LE329	-0.64	1.06	3.731	-13.4	...	5.10	...	1	
L7211	-0.59	1.13	3.513	-29.6	...	5.13	...	1	
W63	-0.53	1.01	3.443	-27.2	...	5.15	...	1	
L8614	-0.52	1.06	3.548	-26.2	...	4.99	...	1	
L5527	-0.51	1.04	3.627	-21.4	...	5.09	...	1	
LE360	-0.49	1.03	3.582	-14.1	...	5.09	...	1	
L1522	-0.47	1.12	3.428	-20.4	...	5.38	...	1	
W193	-0.44	1.05	3.732	-7.8	...	4.96	...	1	
W114	-0.37	1.04	3.473	-20.1	...	4.98	...	1	
L6628	-0.35	1.03	3.463	-30.8	...	4.99	...	1	
L3609	-0.34	1.07	3.540	-15.6	...	5.15	...	1	
L5705/W75	-0.27	1.01	3.509	-16.3	...	4.89	...	1	
L2601	-0.19	0.99	3.445	-13.5	...	4.79	...	1	
L7507	-0.16	1.04	3.375	-20.7	...	4.78	...	1	
L8523	-0.16	1.01	3.407	-25.4	...	4.99	...	1	
L2718	-0.13	0.98	3.421	-16.7	...	4.89	...	1	
L8632	-0.10	0.98	3.196	-21.9	...	4.95	...	1	
L4618	-0.09	0.96	3.077	-13.2	...	4.35	...	1	8,9
L2610	-0.03	0.94	3.520	-14.7	...	4.89	...	1	
L4411	0.07	0.92	3.253	-18.3	...	4.86	...	1	
L5514	0.10	0.92	3.235	-19.2	...	4.93	...	1	
L3513	0.14	0.91	3.286	-14.1	...	4.51	...	1	
L1414	0.17	0.91	3.163	-16.5	...	5.02	...	1	9
L6514	0.20	0.89	3.198	-12.4	...	4.39	...	1	9

TABLE 2. – *continued*

Star	$V - V_{HB}$	$(B - V)_0$	$\log_{10}(\text{Int})$ (e ⁻)	v_r (km s ⁻¹)	$\sigma(v_r)$ (km s ⁻¹)	W(Ca) (Å)	$\sigma(\text{W}(\text{Ca}))$ (Å)	N	Notes
NGC 3201									
108	-2.78	1.36	4.956	498.4	0.4	4.62	0.02	2	10
104	-2.77	1.33	4.977	495.0	0.3	5.03	0.01	2	
098	-2.69	1.24	5.158	495.7	1.3	5.33	0.03	2	
074	-1.92	1.03	4.317	493.2	2.1	4.78	0.01	2	
076	-1.79	1.04	4.637	497.6	0.1	4.53	0.06	2	
085	-1.71	1.14	4.365	500.0	0.9	4.53	0.04	2	
055	-1.40	0.95	4.447	490.7	1.0	4.40	0.06	2	
075	-1.27	1.03	4.199	496.2	...	4.48	...	1	
069	-1.22	1.00	4.231	496.6	...	4.47	...	1	
067	-1.19	1.00	4.207	497.0	...	4.30	...	1	
065	-1.19	0.99	4.153	491.0	...	4.33	...	1	
073	-1.04	1.02	4.105	493.1	...	4.35	...	1	
046	-0.91	0.93	4.546	497.6	1.8	4.04	0.03	2	
060	-0.88	0.97	4.039	489.0	...	4.28	...	1	
034	-0.83	0.89	3.518	496.9	...	3.80	...	1	
028	-0.83	0.86	4.818	491.2	1.2	4.06	0.06	4	
021	-0.64	0.81	4.420	495.4	0.4	3.86	0.16	2	11
037	-0.58	0.90	3.824	489.1	...	4.10	...	1	
035	-0.53	0.89	3.816	494.6	...	4.16	...	1	
030	-0.53	0.87	3.796	496.7	...	3.80	...	1	
043	-0.53	0.92	4.416	494.6	1.1	3.74	0.06	2	
041	-0.49	0.92	4.504	499.1	0.4	3.61	0.03	2	
061	-0.48	0.97	4.693	492.4	0.7	3.99	0.02	3	
042	-0.46	0.92	3.800	495.8	...	4.04	...	1	
054	-0.40	0.94	3.746	500.8	...	4.22	...	1	
020	-0.35	0.81	4.561	488.1	2.2	3.89	0.08	3	
024	-0.35	0.83	4.627	492.7	1.6	3.85	0.05	4	
032	-0.32	0.88	4.690	490.6	0.5	4.02	0.08	4	
029	-0.31	0.87	4.420	491.2	0.6	3.96	0.11	2	
045	-0.26	0.92	3.785	497.5	...	3.93	...	1	
056	-0.25	0.95	3.832	493.4	...	4.18	...	1	
s01	-0.25	0.81	3.741	496.5	...	3.43	...	1	
s07	-0.15	0.78	3.724	493.5	...	3.57	...	1	
s10	-0.14	0.88	3.826	486.5	...	3.74	...	1	
s12	-0.11	0.85	3.411	487.8	...	3.61	...	1	
s14	-0.10	0.85	3.740	498.7	...	3.79	...	1	
s17	-0.08	0.89	3.725	489.6	...	3.88	...	1	
s25	-0.02	0.85	3.803	500.7	...	3.83	...	1	
s32	0.04	0.82	3.730	494.8	...	3.73	...	1	
s34	0.04	0.79	3.641	496.1	...	3.79	...	1	
s38	0.08	0.75	3.633	496.1	...	3.73	...	1	
s43	0.11	0.76	3.508	497.9	...	3.73	...	1	
s48	0.13	0.75	3.717	497.2	...	3.23	...	1	
s64	0.33	0.82	3.017	485.0	...	4.07	...	1	9
s69	0.42	0.73	3.467	497.0	...	3.57	...	1	
s73	0.46	0.75	3.510	492.8	...	3.81	...	1	
s76	0.48	0.86	3.583	498.7	...	3.56	...	1	

TABLE 2. – *continued*

Star	$V - V_{HB}$	$(B - V)_0$	$\log_{10}(\text{Int})$ (e ⁻)	v_r (km s ⁻¹)	$\sigma(v_r)$ (km s ⁻¹)	W(Ca) (Å)	$\sigma(\text{W}(\text{Ca}))$ (Å)	N	Notes
s80	0.52	0.83	3.448	491.8	...	3.63	...	1	
s81	0.52	0.71	3.420	496.8	...	3.60	...	1	
s89	0.61	0.74	2.779	510.4	...	3.24	...	1	9
s94	0.66	0.73	3.362	499.8	...	3.47	...	1	
s95	0.66	0.81	3.295	498.6	...	3.45	...	1	
s106	0.78	0.86	3.473	503.6	...	3.63	...	1	
s107	0.82	0.78	3.259	498.2	...	3.26	...	1	
s109	0.84	0.84	3.393	488.3	...	3.04	...	1	
NGC 6121 (M4)									
1412	-2.97	1.23	4.225	68.7	...	5.05	...	1	7,12
1514	-2.59	1.44	4.281	80.1	...	6.05	...	1	
2406	-2.51	1.29	3.760	73.5	...	5.39	...	1	7,13
4613	-2.50	1.47	4.224	69.5	...	5.70	...	1	
3209	-2.41	1.26	4.021	65.0	...	5.75	...	1	
1411	-2.27	1.35	4.129	69.4	...	5.55	...	1	
3413	-2.02	1.12	3.694	66.3	...	5.43	...	1	
4511	-1.73	1.19	3.961	63.7	...	5.26	...	1	
1501	-1.65	1.13	3.914	72.0	...	5.14	...	1	
4201	-1.64	0.98	3.604	80.8	...	4.62	...	1	10,14
3624	-1.57	1.16	3.461	72.4	...	5.10	...	1	
1408	-1.53	1.01	3.725	73.1	...	4.72	...	1	
2519	-1.53	1.06	3.660	68.8	...	4.98	...	1	
3612	-1.53	1.07	3.737	76.2	...	5.30	...	1	
2617	-1.53	1.20	3.568	65.2	...	4.97	...	1	
2206	-1.45	1.11	3.124	76.4	...	4.86	...	1	9
1403	-1.22	1.06	3.546	71.3	...	4.93	...	1	
1617	-1.17	0.98	3.281	70.2	...	4.78	...	1	
3701	-1.17	0.99	3.488	75.1	...	4.39	...	1	14
2608	-1.10	1.04	3.427	79.1	...	4.87	...	1	
4421	-0.68	0.96	3.314	76.2	...	4.49	...	1	
4416	-0.44	0.94	3.270	76.8	...	4.95	...	1	9
2305	-0.29	0.98	4.423	74.2	1.9	4.40	0.05	2	
3419	-0.28	0.91	2.856	78.1	...	4.29	...	1	9
2404	-0.27	0.90	4.492	67.3	0.8	4.28	0.06	2	
2621	-0.06	0.88	4.338	70.7	0.4	4.14	0.01	2	
1614	0.01	0.89	4.499	69.7	1.1	4.29	0.04	2	
4305	0.11	0.80	4.220	74.1	1.5	4.19	0.16	2	
1506	0.12	0.87	4.302	73.2	0.3	4.08	0.04	2	
1416	0.15	0.86	4.312	71.7	0.6	4.31	0.12	2	
4507	0.17	0.87	4.281	72.7	1.1	4.34	0.07	2	
1621	0.24	0.86	4.229	71.9	2.8	4.22	0.05	2	
3506	0.26	0.86	4.217	70.1	0.8	4.16	0.10	2	
3718	0.32	0.77	4.092	74.3	3.1	4.13	0.04	2	
1402	0.34	0.87	4.374	75.4	0.8	4.20	0.05	2	
4401	0.34	0.89	4.045	75.4	0.8	4.26	0.06	2	
1406	0.49	0.83	4.181	64.8	0.4	4.19	0.01	2	
4623	0.58	0.80	4.186	68.4	2.3	4.10	0.09	2	

TABLE 2. – *continued*

Star	$V - V_{HB}$	$(B - V)_0$	$\log_{10}(\text{Int})$ (e ⁻)	v_r (km s ⁻¹)	$\sigma(v_r)$ (km s ⁻¹)	W(Ca) (Å)	$\sigma(\text{W}(\text{Ca}))$ (Å)	N	Notes
3509	0.62	0.73	4.186	70.8	1.9	4.24	0.16	2	
2712	0.68	0.78	4.007	75.0	2.4	4.22	0.13	2	
3632	0.73	0.82	3.818	65.7	3.0	3.88	0.18	2	
3502	0.90	0.72	3.987	77.2	0.8	4.00	0.19	2	
4514	0.93	0.75	3.939	68.8	2.1	3.99	0.08	2	
4405	0.99	0.74	3.861	64.8	0.5	3.96	0.07	2	
2506	0.98	0.82	3.272	67.6	...	3.61	0.65	2	9
2418	1.00	0.73	4.033	70.9	2.5	3.99	0.17	2	
NGC 6397									
469	-2.94	1.33	4.763	22.0	1.1	4.01	0.01	2	
211	-2.74	1.28	5.286	19.8	0.9	4.06	0.03	2	
603	-2.55	1.15	4.845	26.3	0.1	3.80	0.05	2	
669	-2.40	1.10	4.722	23.2	0.3	3.74	0.07	2	
043	-1.96	0.94	4.935	23.9	0.3	3.40	0.05	2	
428	-1.40	0.87	4.742	19.8	0.6	3.15	0.08	2	
028	-1.09	0.76	4.527	19.6	1.6	2.76	0.09	2	7
685	-0.89	0.79	4.514	20.0	0.1	3.01	0.06	2	
075	-0.78	0.69	4.483	28.9	1.8	2.55	0.10	2	7
025	-0.68	0.78	4.023	15.9	0.1	2.59	0.03	2	
128	-0.66	0.79	4.424	23.0	0.8	2.68	0.09	2	
548	0.12	0.68	4.066	22.7	3.5	2.52	0.07	2	
616	0.28	0.66	3.903	27.5	2.6	2.46	0.04	2	
620	0.29	0.66	3.832	25.2	7.8	2.58	0.16	2	
686	0.60	0.62	3.835	24.5	5.0	2.30	0.08	2	
012	0.68	0.65	3.867	19.5	1.3	2.33	0.16	2	
229	0.89	0.63	3.736	19.5	9.4	2.20	0.04	2	
585	0.90	0.65	3.782	21.2	2.8	2.14	0.02	2	
220	0.94	0.67	3.742	20.5	6.9	2.12	0.03	2	
752	0.99	0.62	3.663	24.1	1.1	2.28	0.14	2	
059	0.99	0.68	3.601	15.4	3.2	2.25	0.03	2	

Notes to TABLE 2.

Notes: 1. Weak TiO present. 2. Possible velocity and photometric variable. 3. Line strength seems to be variable. 4. TiO present. 5. V15. 6. Redward of RGB. 7. AGB star. 8. Spectral line corrupted by cosmic ray. 9. Poor spectrum. 10. Possible AGB star. 11. Line strength inconsistent with color. 12. V4. 13. V13. 14. Lines very weak for photometric position. Also noted in Suntzeff et al. (1993).

TABLE 3A. Photometry, EQW values, and Radial Velocities for ω Cen BG Sample

ROA	$V - V_{HB}$	$(B - V)_0$	R ($^{\circ}$)	$\log_{10}(\text{Int})$ (e $^{-}$)	v_r (km s $^{-1}$)	$\sigma(v_r)$ (km s $^{-1}$)	W(Ca) (\AA)	$\sigma(\text{W}(\text{Ca}))$ (\AA)	[Fe/H] ZW NDC	N	Notes
0040	-3.16	1.35	9.3	5.120	216.7	0.4	4.81	0.03	-1.74 -1.70	3	1
0043	-3.01	1.62	18.0	5.048	235.0	1.1	5.19	0.02	-1.57 -1.55	3	1,2,3
0058	-2.89	1.33	8.4	4.880	235.9	0.4	4.57	0.06	-1.77 -1.72	3	1
0065	-2.97	1.3	6.3	5.058	237.4	0.3	4.56	0.03	-1.79 -1.74	3	4
0074	-2.80	1.28	8.3	4.943	217.7	0.9	4.49	0.04	-1.78 -1.73	3	1
0084	-2.84	1.57	6.0	5.026	218.7	0.8	6.03	0.03	-1.16 -1.23	3	1
0091	-2.73	1.30	14.0	4.866	224.7	0.8	4.53	0.03	-1.75 -1.70	3	1
0095	-2.83	1.43	8.8	4.608	219.1	0.6	5.04	0.03	-1.58 -1.56	3	4
0102	-2.76	1.30	15.6	5.020	247.3	0.6	4.31	0.10	-1.83 -1.77	3	1
0139	-2.64	1.39	9.9	4.894	250.8	1.7	4.92	0.03	-1.58 -1.56	3	1,5
0159	-2.53	1.23	15.3	4.846	229.2	0.2	4.58	0.02	-1.68 -1.65	3	1,6
0162	-2.56	1.55	16.7	4.780	238.2	0.4	5.77	0.04	-1.22 -1.26	3	1,2
0179	-2.66	1.57	6.5	4.954	233.7	0.3	6.41	0.05	-0.80 -1.05	3	1,7
0193	-2.40	1.06	9.1	4.313	237.4	0.6	4.30	0.02	-1.76 -1.71	2	
0206	-2.39	1.07	6.1	4.196	227.5	0.3	4.89	0.06	-1.54 -1.52	2	
0209	-2.37	1.15	11.5	4.393	234.2	0.6	4.17	0.09	-1.80 -1.74	2	1,8,9
0219	-2.48	1.49	15.4	4.365	231.8	0.1	6.01	0.06	-1.01 -1.16	2	
0233	-2.29	1.02	9.8	4.666	230.1	0.8	4.22	0.04	-1.76 -1.71	2	
0234	-2.25	1.05	12.3	4.915	230.8	1.1	4.02	0.10	-1.82 -1.77	5	1,8,10,11
0235	-2.30	1.06	6.1	4.622	235.1	0.1	4.63	0.04	-1.61 -1.59	2	
0236	-2.37	1.34	4.6	4.626	227.4	1.6	5.53	0.04	-1.29 -1.30	2	
0237	-2.34	1.32	3.1	4.451	256.0	0.1	5.30	0.04	-1.37 -1.37	2	
0238	-2.24	1.10	3.6	4.295	257.5	0.4	3.97	0.03	-1.84 -1.78	2	
0239	-2.32	1.22	6.1	4.561	220.1	0.4	5.06	0.01	-1.46 -1.45	2	
0243	-2.36	1.13	7.6	4.746	210.9	0.9	5.62	0.04	-1.24 -1.27	2	
0244	-2.30	1.16	5.3	4.549	260.0	0.5	4.84	0.02	-1.53 -1.52	2	
0245	-2.33	1.25	13.3	4.708	232.9	0.6	5.40	0.08	-1.33 -1.34	2	
0246	-2.19	1.12	6.6	4.452	211.2	0.4	4.38	0.06	-1.68 -1.64	2	
0247	-2.25	1.15	5.5	4.527	246.8	1.6	4.33	0.06	-1.71 -1.67	2	
0248	-2.46	1.66	6.2	4.768	232.4	0.9	5.97	0.07	-1.03 -1.17	3	1
0249	-2.26	1.05	4.5	4.409	235.1	1.1	4.59	0.10	-1.62 -1.59	2	
0251	-2.26	1.24	9.6	4.573	230.8	0.6	4.78	0.01	-1.55 -1.53	2	
0252	-2.22	1.05	14.7	4.941	226.9	1.7	4.17	0.06	-1.76 -1.71	5	
0253	-2.28	1.27	16.7	5.024	232.4	0.8	5.24	0.03	-1.38 -1.38	5	1,6
0254	-2.22	1.06	4.8	4.488	217.8	0.9	4.25	0.04	-1.73 -1.69	2	
0255	-2.24	1.16	8.7	4.588	248.2	0.1	4.51	0.05	-1.64 -1.61	2	
0256	-2.23	1.06	8.7	4.890	229.7	1.0	4.34	0.06	-1.70 -1.66	4	1
0257	-2.20	0.84	8.3	4.536	228.9	0.4	4.10	0.04	-1.78 -1.73	2	
0258	-2.22	0.96	7.4	4.555	243.3	0.7	4.28	0.01	-1.72 -1.68	2	
0259	-2.23	1.00	3.9	4.567	229.6	0.1	4.48	0.06	-1.65 -1.62	2	
0260	-2.25	1.21	10.2	4.613	231.1	1.2	4.74	0.04	-1.56 -1.54	2	
0261	-2.22	1.07	7.4	4.419	238.9	2.1	4.50	0.11	-1.64 -1.61	2	
0262	-2.22	1.05	5.2	4.444	227.9	0.6	4.40	0.04	-1.68 -1.64	2	
0263	-2.27	1.33	3.9	4.374	242.5	0.9	5.14	0.02	-1.42 -1.41	2	
0266	-2.19	1.06	6.2	4.542	239.7	0.3	4.25	0.04	-1.73 -1.68	2	
0267	-2.25	1.29	4.5	4.452	227.4	1.0	5.17	0.02	-1.40 -1.40	2	
0268	-2.18	1.26	6.2	4.413	241.1	0.1	4.36	0.03	-1.68 -1.65	2	

arXiv:astro-ph/9601013v1 4 Jan 1996

TABLE 3A. – *continued*

ROA	$V - V_{HB}$	$(B - V)_0$	R ($^{\circ}$)	$\log_{10}(\text{Int})$ (e $^{-}$)	v_r (km s $^{-1}$)	$\sigma(v_r)$ (km s $^{-1}$)	W(Ca) (\AA)	$\sigma(\text{W}(\text{Ca}))$ (\AA)	[Fe/H]		N	Notes
									ZW	NDC		
0269	-2.19	1.13	12.4	4.644	228.9	0.6	4.43	0.08	-1.66	-1.63	2	1,12
0270	-2.29	1.37	9.9	5.017	240.3	1.2	5.72	0.06	-1.13	-1.22	5	1
0271	-2.18	1.12	11.4	4.637	245.5	0.1	4.42	0.04	-1.66	-1.63	2	
0272	-2.20	1.23	17.9	4.653	239.1	0.4	4.85	0.01	-1.51	-1.49	2	1,12
0275	-2.14	0.89	7.5	4.345	240.1	1.0	3.89	0.01	-1.85	-1.78	2	
0276	-2.30	1.28	5.0	4.480	229.6	0.6	6.40	0.06	-0.64	-0.97	2	13
0277	-2.17	1.08	6.0	4.482	221.4	2.5	4.32	0.06	-1.70	-1.66	2	
0278	-2.17	1.09	7.0	4.331	244.1	2.4	4.36	0.07	-1.68	-1.65	2	
0279	-2.17	1.29	18.0	4.435	236.8	0.7	4.05	0.06	-1.79	-1.74	2	1
0281	-2.19	1.20	6.3	4.437	253.6	1.6	4.68	0.01	-1.57	-1.55	2	
0282	-2.15	1.05	9.1	4.639	229.2	1.8	4.23	0.08	-1.72	-1.68	2	
0285	-2.12	1.03	4.2	4.314	243.6	1.3	3.95	0.00	-1.82	-1.76	2	
0286	-2.25	1.39	4.8	4.248	252.2	0.1	5.90	0.01	-0.98	-1.14	2	14
0287	-2.21	1.31	13.4	4.675	220.4	1.1	5.28	0.06	-1.35	-1.35	2	1,6
0288	-2.13	1.14	8.3	4.507	214.9	1.3	4.18	0.04	-1.74	-1.69	2	
0289	-2.12	1.14	8.7	4.834	261.0	1.3	4.43	0.06	-1.64	-1.61	5	
0290	-2.11	0.96	11.3	4.280	240.3	0.7	4.00	0.00	-1.80	-1.75	2	
0292	-2.11	1.02	4.9	4.374	231.8	0.6	3.96	0.02	-1.81	-1.76	2	
0293	-2.16	1.08	4.5	4.506	231.3	1.4	4.71	0.06	-1.55	-1.53	2	
0296	-2.11	1.07	10.1	4.664	229.8	0.4	4.11	0.04	-1.76	-1.71	2	8,11,12
0300	-2.32	1.40	4.0	4.445	235.0	0.5	6.98	0.00	-0.23	-0.76	2	1,13,15,16
0301	-2.17	1.13	4.8	4.212	213.8	0.1	5.11	0.01	-1.40	-1.40	2	
0302	-2.10	1.08	7.2	4.401	251.5	1.0	4.13	0.13	-1.75	-1.70	2	
0303	-2.08	1.01	7.3	4.427	224.5	0.2	4.02	0.08	-1.79	-1.73	2	
0304	-2.11	0.93	4.2	4.239	214.4	1.7	4.37	0.04	-1.66	-1.63	2	
0308	-2.07	0.99	4.3	4.271	233.6	0.4	4.15	0.03	-1.74	-1.69	2	
0309	-2.05	1.08	3.5	3.846	210.1	0.4	3.83	0.05	-1.85	-1.79	2	
0312	-2.12	1.18	15.8	4.483	223.2	0.9	4.71	0.04	-1.54	-1.52	2	1,8
0313	-2.09	1.09	7.1	4.250	244.2	0.7	4.81	0.04	-1.50	-1.48	2	
0314	-2.11	1.07	3.6	3.989	241.9	0.7	4.84	0.01	-1.49	-1.48	2	
0315	-2.10	1.15	5.6	4.184	239.5	0.4	4.61	0.05	-1.57	-1.55	2	
0316	-2.16	1.48	17.0	4.599	228.4	0.1	6.07	0.06	-0.82	-1.06	2	
0318	-2.04	0.96	4.1	4.302	217.9	0.5	3.99	0.01	-1.79	-1.74	2	
0319	-2.08	1.05	10.0	4.466	224.2	0.1	4.50	0.07	-1.61	-1.58	2	
0320	-1.91	1.53	6.7	4.750	248.1	0.4	4.93	0.03	-1.41	-1.41	2	1,2,16,17,18
0321	-2.21	1.27	5.5	4.350	238.4	1.3	6.09	0.08	-0.83	-1.07	2	
0324	-2.25	1.41	8.3	4.297	239.4	1.0	6.74	0.08	-0.37	-0.83	2	
0325	-2.03	1.06	13.3	4.449	227.1	1.7	4.05	0.01	-1.76	-1.71	2	10
0327	-2.08	1.19	5.2	4.259	218.4	0.8	4.97	0.05	-1.43	-1.43	2	
0328	-2.00	1.10	4.1	4.280	243.7	2.1	3.94	0.06	-1.80	-1.74	2	
0329	-2.07	1.14	4.3	4.249	257.6	0.7	4.83	0.01	-1.48	-1.47	2	
0334	-2.00	0.99	10.4	4.221	229.5	1.2	4.12	0.01	-1.73	-1.69	2	
0336	-2.14	1.29	3.3	4.110	245.1	0.6	5.64	0.11	-1.12	-1.21	2	
0337	-1.99	1.02	7.6	4.273	265.3	0.3	4.00	0.01	-1.77	-1.72	2	
0339	-2.07	1.16	9.7	4.415	226.2	0.7	5.14	0.02	-1.37	-1.37	2	
0341	-2.06	1.19	9.9	4.538	245.4	1.8	4.99	0.11	-1.42	-1.42	2	
0342	-1.94	0.57	12.1	3.795	240.9	2.1	3.42	0.01	-1.97	-1.89	2	21

TABLE 3A. – *continued*

ROA	$V - V_{HB}$	$(B - V)_0$	R ($^{\circ}$)	$\log_{10}(\text{Int})$ (e $^{-}$)	v_r (km s $^{-1}$)	$\sigma(v_r)$ (km s $^{-1}$)	W(Ca) (\AA)	$\sigma(\text{W}(\text{Ca}))$ (\AA)	[Fe/H]		N	Notes
									ZW	NDC		
0343	-1.97	0.95	2.9	3.935	234.0	0.9	3.85	0.17	-1.82	-1.76	2	
0344	-2.03	1.06	5.5	4.186	237.1	3.5	4.67	0.04	-1.53	-1.52	2	
0345	-2.05	1.27	6.3	4.254	225.4	0.1	4.92	0.03	-1.45	-1.44	2	
0348	-1.99	1.02	9.1	4.482	232.5	1.4	4.22	0.04	-1.69	-1.65	2	
0350	-1.97	0.87	5.6	4.143	209.8	1.0	3.88	0.01	-1.81	-1.76	2	
0351	-1.98	0.99	10.3	4.335	248.9	0.4	4.19	0.06	-1.70	-1.66	2	
0352	-2.06	1.13	8.7	4.149	237.5	0.3	5.23	0.01	-1.33	-1.34	2	
0355	-1.96	0.97	7.4	4.308	248.3	1.4	3.96	0.02	-1.78	-1.73	2	
0356	-1.96	0.97	3.6	4.204	262.8	0.3	3.93	0.06	-1.79	-1.74	2	
0357	-2.25	1.1	5.8	4.258	228.1	1.2	6.69	0.06	-0.41	-0.85	2	1,4,19
0359	-2.00	1.18	12.9	4.296	235.4	2.3	4.81	0.11	-1.48	-1.47	2	8
0361	-1.96	1.07	8.7	4.331	232.4	0.8	4.25	0.01	-1.67	-1.64	2	10
0362	-1.96	0.99	9.3	4.265	240.8	3.1	4.09	0.05	-1.73	-1.69	2	
0364	-1.95	1.01	8.0	4.325	238.6	3.9	4.03	0.11	-1.75	-1.71	2	1,14
0367	-2.13	1.35	7.8	4.369	228.2	1.2	5.72	0.01	-1.06	-1.18	2	
0368	-1.95	1.05	7.1	4.312	239.0	1.3	3.99	0.02	-1.77	-1.72	2	
0371	-2.12	1.53	8.9	4.718	226.6	0.2	6.71	0.18	-0.33	-0.81	4	1,2,13,20
0372	-2.03	1.28	5.0	4.226	225.0	1.2	5.36	0.11	-1.28	-1.29	2	
0373	-1.91	0.95	7.1	4.070	216.6	0.6	3.92	0.05	-1.78	-1.73	2	
0375	-1.90	0.87	6.6	4.173	237.6	2.8	3.82	0.04	-1.82	-1.76	2	
0376	-1.98	1.21	6.2	4.254	247.4	1.6	5.01	0.09	-1.40	-1.40	2	
0377	-1.90	0.97	10.3	4.192	219.8	0.4	4.06	0.00	-1.73	-1.69	2	
0378	-1.94	1.19	12.6	4.736	222.9	0.8	4.84	0.04	-1.45	-1.44	4	8
0379	-1.92	1.09	10.9	4.314	237.1	1.8	4.22	0.05	-1.67	-1.64	2	
0380	-1.92	1.11	8.9	4.238	237.7	0.4	4.37	0.05	-1.62	-1.59	2	8,14
0382	-1.91	0.97	5.2	4.148	245.9	0.5	4.26	0.08	-1.66	-1.63	2	
0383	-1.81	1.15	4.4	3.452	251.6	3.7	2.95	0.04	-2.12	-2.00	2	21
0385	-1.88	1.04	6.3	3.990	235.4	2.3	4.01	0.15	-1.74	-1.70	2	
0386	-2.02	1.36	5.7	4.084	231.2	1.0	5.94	0.00	-0.85	-1.08	2	
0387	-1.85	1.01	12.5	4.129	226.8	1.6	3.76	0.04	-1.83	-1.77	2	
0389	-1.91	1.14	16.2	4.179	238.6	1.1	4.54	0.01	-1.55	-1.54	2	
0390	-1.88	0.99	6.0	4.053	234.5	0.2	4.19	0.06	-1.68	-1.64	2	
0391	-1.85	0.81	4.1	4.013	226.1	2.3	3.74	0.00	-1.84	-1.78	2	
0392	-1.87	0.99	2.9	4.012	224.1	0.6	4.04	0.04	-1.73	-1.69	2	
0394	-2.01	1.25	19.0	3.787	228.0	0.6	5.55	0.02	-1.13	-1.22	2	1,6
0395	-1.90	1.11	10.7	4.049	251.9	0.1	4.52	0.08	-1.56	-1.54	2	
0396	-1.93	1.04	18.5	4.218	222.1	0.4	4.93	0.02	-1.42	-1.41	2	
0397	-1.85	0.97	5.1	3.933	238.4	2.4	3.85	0.13	-1.80	-1.74	2	
0402	-1.85	0.97	13.8	4.056	237.8	0.7	3.94	0.05	-1.76	-1.71	2	1
0405	-1.89	1.04	4.9	4.005	239.8	1.9	4.69	0.16	-1.49	-1.48	2	
0406	-1.86	1.09	4.0	4.147	230.8	0.6	4.24	0.08	-1.65	-1.62	2	
0407	-1.90	1.11	10.0	4.104	235.1	0.2	5.18	0.05	-1.32	-1.32	2	8,9
0408	-1.84	0.92	11.8	4.086	244.5	0.5	4.05	0.01	-1.72	-1.68	2	
0410	-1.81	0.97	4.2	3.987	247.2	3.5	3.69	0.04	-1.85	-1.78	2	
0417	-1.85	1.13	7.8	4.002	237.3	0.7	4.51	0.03	-1.55	-1.53	2	
0418	-1.80	1.02	12.1	3.978	226.6	1.8	3.88	0.04	-1.77	-1.72	2	12
0419	-1.89	1.25	3.5	3.966	254.0	1.7	5.15	0.06	-1.32	-1.33	2	

TABLE 3A. – *continued*

ROA	$V - V_{HB}$	$(B - V)_0$	R ($^{\circ}$)	$\log_{10}(\text{Int})$ (e $^{-}$)	v_r (km s $^{-1}$)	$\sigma(v_r)$ (km s $^{-1}$)	W(Ca) (\AA)	$\sigma(\text{W}(\text{Ca}))$ (\AA)	[Fe/H]		N	Notes
									ZW	NDC		
0421	-1.94	1.32	4.5	3.797	233.4	0.8	6.20	0.02	-0.62	-0.96	2	1
0429	-1.75	0.98	4.3	3.995	226.6	0.1	3.44	0.16	-1.92	-1.85	2	21
0433	-1.84	1.17	4.0	4.050	234.4	0.2	4.72	0.13	-1.47	-1.46	2	
0434	-1.81	1.06	20.3	4.145	234.5	2.3	4.41	0.08	-1.58	-1.56	2	6
0435	-1.72	0.96	18.0	3.572	225.1	5.9	3.26	0.01	-1.98	-1.89	2	21
0436	-1.81	1.01	4.1	3.919	228.0	3.0	4.42	0.05	-1.58	-1.56	2	
0443	-1.72	1.07	3.3	3.883	246.1	1.7	3.70	0.26	-1.82	-1.76	2	
0444	-1.81	1.21	5.1	3.917	234.0	0.3	4.85	0.23	-1.42	-1.41	2	
0445	-1.80	1.19	6.6	3.810	258.8	2.2	4.79	0.07	-1.44	-1.43	2	
0446	-1.76	1.00	14.8	4.099	252.9	0.1	4.07	0.05	-1.69	-1.66	2	10,11,12
0447	-1.93	1.58	10.2	4.508	225.5	0.7	7.07	0.08	-0.25	-0.62	2	1,7,16
0448	-1.72	0.92	13.7	3.925	237.7	2.4	3.72	0.01	-1.81	-1.76	2	
0449	-1.74	1.02	13.0	3.992	232.5	0.9	4.04	0.14	-1.70	-1.66	2	
0462	-1.72	0.86	8.8	4.502	235.6	2.4	3.61	0.14	-1.85	-1.79	4	1
0464	-1.70	1.08	15.7	3.929	227.4	1.6	4.07	0.21	-1.68	-1.65	2	1
0470	-1.71	0.93	12.2	3.717	238.0	2.4	3.93	0.19	-1.73	-1.69	2	10
0476	-1.72	0.94	19.1	3.914	244.3	0.3	3.92	0.12	-1.74	-1.70	2	
0480	-1.87	1.33	6.0	4.400	229.4	0.8	5.93	0.07	-0.79	-1.05	3	1
0483	-1.70	0.96	15.6	3.865	245.9	0.8	3.74	0.15	-1.80	-1.75	2	1,12
0484	-1.72	1.11	21.5	3.993	232.5	0.2	4.06	0.15	-1.69	-1.65	2	

Notes to TABLE 3a.

1. *JHK* photometry in Persson et al. (1980).
2. Variable according to Cannon & Stobie (1973).
3. Variable according to Persson, et al. (1980).
4. Photometry quite discrepant among sources. Probably variable.
5. Eggen photometry quoted in Bessell & Norris (1976).
6. Alcaino & Liller (1984).
7. Probable TiO. Lloyd Evans (1983a,b).
8. Martin (1981).
9. Possible continuation of photometry from nearby star.
10. Photometry from Hesser et al. (1977).
11. Average of all secondary photometry.
12. Hawarden & Epps Bingham (1987) photometry.
13. Photometry in Llyod Evans (1983a) differs by 0.1 mag. Possible variable or bad photometry.
14. Crowded. Photometry uncertain in Llyod Evans (1983a).
15. Possible TiO (Lloyd Evans 1983a).
16. S star according to Lloyd Evans (1983b).
17. TiO variable, according to Dickens et al. (1972).
18. Variable in Lloyd Evans (1983a). $V = 12.00, 12.57, 12.85$.
19. V photometry quite discrepant in Lloyd Evans (1983a).
20. No M or S star features according to Lloyd Evans (1983b).
21. Possible AGB star based on line strengths (see text).

TABLE 3B. Photometry, EQW values, and Radial Velocities for ω Cen SG Sample

ROA	$V - V_{HB}$	$(B - V)_0$	R ($^{\circ}$)	$\log_{10}(\text{Int})$ (e $^{-}$)	v_r (km s $^{-1}$)	$\sigma(v_r)$ (km s $^{-1}$)	W(Ca) (\AA)	$\sigma(\text{W}(\text{Ca}))$ (\AA)	[Fe/H]		N	Notes
									ZW	NDC		
1031	0.30	0.83	20.8	3.926	244.0	1.3	3.63	0.08	-1.48	-1.47	2	1
1109	0.22	0.75	19.4	3.947	230.9	0.1	3.54	0.02	-1.53	-1.51	2	
1164	0.50	0.77	19.4	2.816	227.6	4.5	4.21	0.64	-1.21	-1.25	2	2
1184	0.32	0.67	17.6	3.947	235.4	0.6	3.04	0.12	-1.70	-1.66	2	
1215	0.30	0.65	17.9	3.926	233.9	2.0	2.89	0.06	-1.76	-1.71	2	
1257	0.62	0.77	19.5	3.652	242.5	1.4	2.86	0.10	-1.73	-1.69	2	
1284	0.71	0.70	15.6	3.625	259.0	4.9	3.04	...	-1.65	-1.62	2	
1317	0.46	0.68	16.0	3.857	236.8	1.4	2.51	0.01	-1.88	-1.81	2	
1327	0.62	0.68	16.7	3.812	225.4	4.9	2.68	0.18	-1.79	-1.74	2	
1342	0.48	0.70	17.2	3.592	241.6	5.3	2.96	0.58	-1.71	-1.67	2	
1360	0.26	0.66	18.1	3.481	216.2	6.2	3.19	0.06	-1.65	-1.62	2	
1391	0.51	0.50	21.1	3.742	219.4	1.1	3.54	0.23	-1.49	-1.48	2	
1415	0.65	0.68	19.8	3.803	228.0	3.0	3.83	0.19	-1.37	-1.37	2	
1424	0.44	0.46	16.7	3.538	236.8	0.1	2.74	0.16	-1.80	-1.74	2	
1472	0.67	0.82	13.8	3.732	241.6	0.4	3.51	0.24	-1.48	-1.47	2	
1473	0.39	0.75	12.9	3.374	228.6	8.1	3.55	0.28	-1.50	-1.49	2	
1480	0.74	0.74	12.6	3.714	249.1	1.8	2.90	0.06	-1.70	-1.66	2	
1510	0.58	0.70	13.0	3.578	226.5	...	2.62	0.28	-1.82	-1.76	2	
1511	0.74	0.78	13.4	3.713	212.4	0.4	2.63	0.04	-1.80	-1.74	2	
1515	0.66	0.62	13.1	3.453	264.0	8.6	2.40	0.05	-1.89	-1.82	2	
1518	0.51	0.74	14.4	3.588	232.4	3.1	2.87	0.09	-1.74	-1.69	2	
1602	0.65	0.90	16.6	3.742	222.1	4.9	4.03	0.23	-1.29	-1.30	2	
1610	0.50	0.75	14.6	3.625	235.8	3.3	2.90	0.18	-1.73	-1.69	2	
1657	0.64	0.71	12.6	3.540	237.6	5.2	2.87	0.09	-1.72	-1.68	2	
1665	0.60	0.74	12.8	3.322	250.7	1.6	2.82	0.60	-1.74	-1.70	2	
1772	0.30	0.71	12.5	2.766	217.6	4.5	3.41	1.0:	-1.57:	-1.55	2	
1780	0.75	0.74	13.0	3.717	246.2	0.5	2.68	0.06	-1.78	-1.73	2	
1783	0.35	0.68	12.9	3.506	224.4	10.7	2.87	0.13	-1.76	-1.71	2	
1786	0.47	0.88	12.7	3.531	244.5	1.9	3.65	0.40	-1.46	-1.45	2	
1793	0.71	0.56	14.0	3.597	239.2	5.5	3.12	0.28	-1.62	-1.59	2	3
1834	0.75	0.74	18.5	3.753	245.9	2.7	2.72	0.18	-1.76	-1.71	2	
1895	0.49	0.76	11.2	3.414	236.1	1.8	2.55	0.05	-1.86	-1.79	2	
1912	0.53	0.78	9.7	3.416	233.6	6.0	4.05	0.24	-1.30	-1.31	2	
1920	0.51	0.75	9.6	3.604	214.1	8.6	2.61	0.13	-1.83	-1.77	2	
1927	0.43	0.72	10.0	3.600	221.9	2.1	2.54	0.28	-1.87	-1.80	2	
1928	0.20	0.84	9.6	3.699	216.9	6.1	4.25	0.48	-1.26	-1.28	4	
1933	0.75	0.85	10.0	3.337	236.9	5.4	2.52	0.33	-1.84	-1.78	2	
1966	0.43	0.68	10.8	3.363	234.2	4.9	2.68	0.01	-1.82	-1.76	2	
1975	0.71	0.72	11.2	3.668	236.4	8.3	3.01	0.18	-1.66	-1.63	2	
1980	0.11	0.93	12.1	3.470	225.1	1.1	4.65	...	-0.99	-1.15	2	4
2061	0.29	0.74	10.3	3.609	210.6	6.8	2.86	0.18	-1.77	-1.72	2	
2063	0.27	0.86	10.8	3.469	216.8	4.5	4.39	...	-1.14	-1.22	2	
2068	0.30	0.78	10.0	3.732	241.1	2.5	2.84	0.01	-1.78	-1.73	2	
2097	0.33	0.70	9.3	2.834	237.6	1.8	2.69	0.33	-1.83	-1.77	2	
2112	0.61	0.74	9.0	3.600	230.4	5.2	2.82	0.05	-1.74	-1.70	2	
2139	0.70	0.77	9.2	3.566	248.4	7.1	2.89	0.21	-1.71	-1.67	2	
2147	0.64	0.79	9.4	3.331	227.6	3.4	3.00	...	-1.67	-1.64	2	

TABLE 3B. – *continued*

ROA	$V - V_{HB}$	$(B - V)_0$	R ($'$)	$\log_{10}(\text{Int})$ (e^-)	v_r (km s^{-1})	$\sigma(v_r)$ (km s^{-1})	W(Ca) (\AA)	$\sigma(W(\text{Ca}))$ (\AA)	[Fe/H]		N	Notes
									ZW	NDC		
2155	0.56	0.64	10.0	3.675	225.8	5.4	2.66	0.45	-1.81	-1.75	2	
2191	0.37	0.79	13.8	3.561	239.0	0.1	2.52	0.04	-1.89	-1.82	2	
2200	0.42	0.70	16.7	3.558	227.7	3.8	2.87	0.16	-1.75	-1.70	2	
2209	0.31	0.67	22.4	3.638	236.0	1.6	2.86	0.13	-1.77	-1.72	2	
2256	0.31	0.69	9.9	2.876	225.8	0.9	2.97	0.06	-1.73	-1.68	2	
2257	0.65	0.72	9.8	3.436	233.7	0.7	2.78	0.14	-1.75	-1.71	2	
2278	0.25	0.95	8.0	3.560	214.4	1.5	3.91	0.24	-1.39	-1.39	2	
2291	0.36	0.92	7.8	2.894	225.2	3.4	2.14	0.13	-2.03	-1.93	2	
2292	0.54	0.77	7.6	3.470	239.5	4.8	3.00	0.26	-1.69	-1.65	2	
2310	0.57	0.66	9.0	3.563	227.6	0.1	2.60	0.15	-1.83	-1.77	2	
2332	0.50	0.82	9.6	3.423	233.1	7.4	2.77	0.12	-1.78	-1.73	2	
2337	0.71	0.68	9.8	3.494	241.2	0.3	3.06	0.30	-1.64	-1.61	2	
2340	0.74	0.70	10.3	3.656	240.4	5.7	3.12	0.23	-1.62	-1.59	2	
2341	0.45	0.72	9.9	3.715	249.4	3.6	3.85	0.14	-1.38	-1.38	2	
2362	0.29	0.75	13.3	3.718	254.6	4.7	2.92	0.12	-1.75	-1.70	2	
2373	0.45	0.74	16.0	3.617	225.0	1.4	2.76	0.16	-1.79	-1.73	2	
2383	0.62	0.74	21.6	3.568	234.4	7.4	2.95	0.12	-1.69	-1.66	2	
2424	0.41	0.78	9.5	3.586	241.2	8.6	2.97	0.01	-1.71	-1.67	2	
2439	0.73	0.68	8.7	3.373	235.1	1.0	2.26	0.01	-1.93	-1.85	2	
2532	0.49	0.79	9.7	3.639	233.9	13.6	3.04	0.06	-1.68	-1.64	2	
2555	0.34	0.82	11.5	3.074	259.0	5.0	2.79	0.35	-1.79	-1.74	2	
2769	0.41	0.70	10.2	3.671	244.3	4.2	2.85	0.01	-1.76	-1.71	2	
2777	0.30	0.80	11.3	3.632	250.9	5.8	3.81	0.04	-1.42	-1.41	2	
2779	0.38	0.72	11.8	3.559	249.2	9.7	2.81	0.08	-1.78	-1.73	2	
2789	0.42	0.71	13.8	3.586	233.5	3.3	2.85	0.11	-1.76	-1.71	2	
2809	0.30	0.89	14.0	3.476	238.7	0.0	3.83	0.04	-1.41	-1.41	2	
2840	0.59	0.84	8.7	3.402	210.7	2.4	3.05	0.21	-1.66	-1.63	2	
3072	0.27	0.76	21.6	3.632	238.5	2.5	4.02	0.23	-1.34	-1.35	2	
3082	0.38	0.90	14.5	3.585	219.1	2.3	3.47	0.06	-1.53	-1.52	2	
3085	0.40	0.86	13.9	3.577	224.6	0.0	3.38	0.26	-1.56	-1.54	2	
3104	0.25	0.74	11.0	2.944	232.4	4.9	4.05	0.99	-1.34	-1.34	2	
3350	0.72	0.84	13.7	3.496	226.4	4.2	2.94	0.18	-1.69	-1.65	2	
3383	0.23	0.91	16.0	3.035	212.1	0.4	4.37	0.06	-1.16	-1.23	2	5
3386	0.50	0.74	15.2	3.604	221.7	5.5	3.57	0.07	-1.48	-1.47	2	5
3393	0.16	0.92	13.4	3.529	224.3	3.3	4.47	0.13	-1.11	-1.20	2	
3396	0.43	0.78	11.4	3.552	225.1	6.9	3.46	0.35	-1.53	-1.52	2	
3417	0.73	0.63	8.7	3.382	216.6	11.2	3.05	0.26	-1.64	-1.61	2	
3608	0.65	0.76	11.9	3.549	237.0	1.8	3.01	0.60	-1.67	-1.64	2	
3620	0.61	0.74	16.6	3.740	245.1	0.8	4.29	0.04	-1.12	-1.21	2	
3633	0.73	0.64	21.7	3.779	251.9	5.8	2.67	0.21	-1.78	-1.73	2	3
3660	0.68	0.90	10.6	3.671	247.6	6.0	3.46	0.12	-1.50	-1.49	2	
3830	0.66	0.79	8.8	3.568	234.9	2.8	2.70	0.09	-1.78	-1.73	2	
3897	0.22	0.80	12.4	3.572	234.1	1.6	4.27	0.25	-1.24	-1.27	2	
3901	0.29	0.89	11.7	3.723	216.7	1.1	4.76	0.09	-0.86	-1.08	2	
3917	0.39	0.73	9.1	3.482	224.3	10.5	3.22	0.26	-1.62	-1.60	2	
3927	0.44	0.82	8.6	3.622	211.4	0.4	3.26	0.42	-1.60	-1.58	2	
4100	0.43	0.66	9.0	3.556	241.9	0.1	3.43	0.25	-1.54	-1.53	2	6

TABLE 3B. – *continued*

ROA	$V - V_{HB}$	$(B - V)_0$	R ($'$)	$\log_{10}(\text{Int})$ (e $^-$)	v_r (km s $^{-1}$)	$\sigma(v_r)$ (km s $^{-1}$)	W(Ca) (\AA)	$\sigma(W(\text{Ca}))$ (\AA)	[Fe/H]		N	Notes
									ZW	NDC		
4118	0.38	0.86	13.4	3.548	243.4	5.9	2.96	0.07	-1.72	-1.68	2	
4130	0.59	0.72	17.8	3.640	239.8	0.2	2.70	0.06	-1.79	-1.74	2	
4185	0.47	0.76	9.1	3.598	225.0	1.6	3.50	0.03	-1.51	-1.50	2	
4384	0.17	0.76	14.5	3.081	232.9	3.3	4.52	0.30	-1.07	-1.19	2	
4416	0.67	0.74	13.8	3.563	246.9	8.5	2.65	0.15	-1.80	-1.74	2	
4432	0.61	0.74	10.8	3.514	224.5	0.2	3.05	0.33	-1.66	-1.63	2	
4440	0.23	0.83	10.1	3.672	235.5	2.1	3.55	0.25	-1.52	-1.51	2	
4456	0.43	0.78	8.7	3.463	225.6	4.8	3.19	...	-1.63	-1.60	2	
4636	0.57	0.72	12.8	3.665	238.1	2.5	3.34	0.02	-1.56	-1.54	2	
4663	0.36	0.76	16.7	3.065	241.8	4.6	2.51	0.08	-1.89	-1.82	2	7
4667	0.50	0.81	13.8	3.748	222.1	1.3	2.97	0.11	-1.70	-1.66	2	
4675	0.70	0.67	11.2	3.778	222.0	1.1	2.84	0.06	-1.72	-1.68	2	
4684	0.60	0.76	10.7	3.630	225.7	0.3	2.62	0.19	-1.82	-1.76	2	
4703	0.75	0.66	8.8	3.712	233.5	0.6	2.45	0.13	-1.86	-1.80	2	
4955	0.61	0.72	9.9	3.551	239.6	...	3.09	...	-1.64	-1.61	2	
4960	0.55	0.79	10.2	3.575	240.2	4.2	3.06	0.18	-1.66	-1.63	2	
4979	0.50	0.84	13.2	3.617	239.6	8.0	4.10	0.21	-1.29	-1.29	2	
4984	0.76	0.70	15.0	3.712	228.3	4.0	2.87	0.10	-1.71	-1.67	2	
4985	0.69	0.76	15.1	3.468	248.4	2.3	3.07	0.47	-1.64	-1.61	2	
4996	0.32	0.57	19.1	3.060	236.7	4.5	3.32	0.14	-1.60	-1.57	2	
5017	0.40	0.93	15.2	3.704	226.0	2.4	4.83	0.06	-0.78	-1.04	2	
5026	0.27	0.70	11.9	3.619	243.9	4.4	2.92	0.13	-1.75	-1.70	2	
5057	0.64	0.86	8.4	3.656	233.4	0.9	4.06	0.35	-1.28	-1.29	2	
5263	0.31	0.85	9.0	3.603	239.4	8.4	3.68	0.31	-1.47	-1.46	2	
5266	0.42	0.86	9.0	3.580	249.5	5.9	4.06	0.14	-1.31	-1.32	2	
5286	0.57	0.77	12.8	3.695	225.9	3.7	2.72	0.30	-1.79	-1.73	2	
5335	0.24	0.89	12.1	3.502	224.9	5.1	3.35	0.01	-1.60	-1.57	2	
5343	0.41	0.76	10.7	3.499	225.7	6.2	2.58	0.17	-1.86	-1.79	2	
5344	0.29	0.79	10.7	3.074	207.4	19.7	2.82	0.31	-1.78	-1.73	2	
5356	0.35	0.81	9.7	3.184	219.2	4.5	4.73	0.74	-0.87	-1.09	2	
5507	0.34	0.70	8.9	2.955	224.2	6.5	3.05	0.14	-1.69	-1.66	2	
5508	0.59	0.77	9.0	3.643	245.4	3.0	3.26	0.17	-1.58	-1.56	2	
5509	0.66	0.84	9.5	3.705	232.4	2.8	3.02	0.31	-1.66	-1.63	2	
5514	0.67	0.77	9.9	3.552	229.9	7.5	2.82	0.06	-1.74	-1.69	2	
5520	0.45	0.75	10.4	3.791	237.4	1.5	3.81	0.04	-1.40	-1.40	2	
5531	0.76	0.75	11.3	4.059	249.7	2.1	2.80	0.06	-1.73	-1.69	4	
5600	0.30	0.79	9.7	3.622	219.3	2.5	5.02	0.25	-0.67	-0.99	2	
5605	0.33	0.79	9.1	3.129	230.5	17.0	3.58	0.54	-1.50	-1.49	2	
5612	0.53	0.72	8.7	3.647	226.1	1.3	4.08	0.06	-1.29	-1.30	2	
5617	0.53	0.83	8.6	3.611	214.5	4.0	2.99	0.06	-1.69	-1.65	2	
5689	0.43	0.81	8.5	3.434	232.1	0.6	5.02	0.09	-0.64	-0.97	2	
5692	0.55	0.90	8.4	3.502	235.6	1.6	3.48	0.03	-1.51	-1.50	2	
5702	0.46	0.80	9.4	3.584	250.2	2.5	2.86	0.02	-1.75	-1.70	2	
5704	0.52	0.77	10.0	3.666	248.6	...	2.56	...	-1.85	-1.79	2	
5705	0.35	0.73	9.8	3.469	234.5	3.7	3.92	0.16	-1.37	-1.37	2	
5721	0.66	0.84	12.6	3.611	248.4	2.4	2.76	0.50	-1.76	-1.71	2	
5737	0.51	0.77	17.0	3.675	237.1	3.8	3.33	0.06	-1.57	-1.55	2	

TABLE 3B. – *continued*

ROA	$V - V_{HB}$	$(B - V)_0$	R ($'$)	$\log_{10}(\text{Int})$ (e^-)	v_r (km s^{-1})	$\sigma(v_r)$ (km s^{-1})	W(Ca) (\AA)	$\sigma(W(\text{Ca}))$ (\AA)	[Fe/H]		N	Notes
									ZW	NDC		
5763	0.29	0.86	13.6	3.471	231.0	1.7	3.75	0.11	-1.44	-1.44	2	
5769	0.30	0.81	12.5	2.861	238.5	3.0	2.92	0.23	-1.75	-1.70	2	
5874	0.42	0.65	8.7	3.589	241.9	8.1	2.86	0.25	-1.75	-1.71	2	
5885	0.66	0.77	10.1	3.589	225.9	1.6	3.36	0.21	-1.54	-1.52	2	
5926	0.23	0.80	18.9	3.691	218.1	2.1	3.79	0.07	-1.43	-1.43	2	
5953	0.53	0.72	15.9	3.622	230.5	4.8	3.07	0.10	-1.66	-1.63	2	
5972	0.58	0.77	10.7	3.206	227.8	0.6	2.66	0.18	-1.81	-1.75	2	
5986	0.51	0.79	9.3	3.199	235.4	6.4	2.75	0.40	-1.78	-1.73	2	
5998	0.46	0.76	8.2	3.531	225.3	0.1	3.26	0.20	-1.60	-1.58	2	
6046	0.31	0.84	8.5	3.441	233.1	3.6	4.20	0.21	-1.27	-1.28	2	
6063	0.49	0.73	10.2	3.481	230.3	4.2	2.70	0.19	-1.80	-1.75	2	
6110	0.33	0.77	18.1	3.662	225.6	1.1	4.37	0.13	-1.14	-1.22	2	1
6151	0.48	0.83	9.7	3.462	215.5	3.7	2.65	0.16	-1.82	-1.76	2	
6157	0.25	0.85	9.4	2.933	230.1	3.3	4.08	0.24	-1.33	-1.33	2	
6165	0.53	0.69	8.7	3.595	231.6	...	2.92	...	-1.72	-1.68	2	
6190	0.73	0.79	9.4	3.623	230.6	9.8	2.18	0.07	-1.96	-1.88	2	
6199	0.27	0.81	9.1	3.403	235.6	1.1	3.15	0.11	-1.67	-1.63	2	
6252	0.32	0.74	14.9	2.513	241.6	2.9	2.74	1.0:	-1.81:	-1.75	2	
6255	0.55	0.80	14.2	3.497	233.0	5.7	2.56	0.25	-1.85	-1.78	2	
6274	0.49	0.90	11.6	3.170	229.5	12.9	2.61	0.23	-1.84	-1.78	2	
6287	0.33	0.71	10.7	3.450	226.6	3.7	3.13	0.22	-1.67	-1.63	2	
6321	0.54	0.80	9.7	3.485	239.1	0.8	2.37	0.11	-1.92	-1.84	2	
6326	0.46	0.83	10.0	3.505	221.5	4.7	3.65	0.40	-1.46	-1.45	2	6
6333	0.23	0.78	10.7	2.986	229.6	5.9	3.71	0.20	-1.46	-1.46	2	
6335	0.70	0.85	10.6	3.647	220.8	2.3	3.03	0.16	-1.65	-1.62	2	
6354	0.32	0.77	13.2	2.792	234.4	19.2	2.58	0.56	-1.87	-1.80	2	
6360	0.52	0.71	13.8	3.667	231.1	0.6	3.04	0.05	-1.67	-1.64	2	
6361	0.31	0.79	14.1	3.115	237.4	9.8	2.99	0.08	-1.72	-1.68	2	
6372	0.46	0.68	16.4	3.581	248.4	0.4	3.74	0.04	-1.42	-1.42	2	
6390	0.61	0.70	19.5	3.551	233.8	4.5	2.55	0.01	-1.84	-1.78	2	
6395	0.67	0.81	16.4	3.787	213.4	2.5	3.07	0.11	-1.64	-1.61	2	
6433	0.61	0.67	12.4	3.723	233.1	4.8	3.80	0.11	-1.38	-1.38	2	
6440	0.46	0.70	11.8	3.417	228.6	13.9	2.30	0.18	-1.95	-1.87	2	
6441	0.56	0.65	12.9	3.499	230.1	1.3	2.83	0.06	-1.75	-1.70	2	
6454	0.66	0.67	12.1	3.406	234.4	4.4	2.59	0.18	-1.82	-1.76	2	
6456	0.47	0.72	11.8	3.477	234.2	8.7	2.92	0.31	-1.72	-1.68	2	
6462	0.43	0.71	11.6	3.504	221.9	5.7	3.00	0.35	-1.70	-1.66	2	
6467	0.76	0.73	11.4	3.670	257.6	9.8	2.54	0.11	-1.83	-1.77	2	
6480	0.66	0.69	11.4	3.378	231.3	6.4	2.77	0.35	-1.76	-1.71	2	
6496	0.61	0.67	11.0	3.559	240.8	3.2	2.88	0.07	-1.72	-1.68	2	
6518	0.57	0.66	12.3	3.697	228.3	4.0	3.26	0.25	-1.59	-1.56	2	
6531	0.33	0.63	13.0	3.397	231.8	1.8	2.74	0.01	-1.81	-1.75	2	
6552	0.27	0.75	14.4	3.640	243.6	1.3	2.99	0.30	-1.72	-1.68	2	
6553	0.51	0.75	14.5	3.658	233.1	0.5	3.23	0.06	-1.61	-1.58	2	
6626	0.58	0.72	15.8	3.608	241.8	3.1	3.95	0.14	-1.33	-1.33	2	3
6644	0.72	0.68	14.9	3.547	243.9	2.4	2.94	0.18	-1.69	-1.65	2	
6656	0.59	0.70	13.7	3.543	221.0	4.4	2.76	0.07	-1.77	-1.72	2	

TABLE 3B. – *continued*

ROA	$V - V_{HB}$	$(B - V)_0$	R ($'$)	$\log_{10}(\text{Int})$ (e $-$)	v_r (km s $^{-1}$)	$\sigma(v_r)$ (km s $^{-1}$)	W(Ca) (\AA)	$\sigma(\text{W(Ca)})$ (\AA)	[Fe/H]		N	Notes
									ZW	NDC		
6740	0.51	0.66	17.3	3.617	225.0	0.7	3.15	0.16	-1.63	-1.61	2	
6766	0.35	0.78	15.2	3.334	244.4	6.9	3.22	0.18	-1.63	-1.60	2	
6776	0.42	0.77	14.9	3.560	227.3	2.4	3.55	0.00	-1.50	-1.49	2	
6781	0.55	0.81	15.0	3.441	225.0	3.3	3.07	0.04	-1.66	-1.63	2	
6784	0.38	0.76	14.4	3.597	213.7	9.2	2.76	0.25	-1.80	-1.74	4	
6796	0.74	0.69	15.0	3.613	232.5	4.0	2.94	0.16	-1.68	-1.65	2	
6807	0.32	0.57	16.1	2.919	237.7	11.6	3.04	0.62	-1.70	-1.66	2	
6811	0.68	0.74	15.6	3.718	244.9	2.9	2.88	0.21	-1.71	-1.67	2	
6822	0.45	0.71	18.1	3.484	231.4	2.9	3.47	0.18	-1.52	-1.51	2	
6827	0.48	0.60	17.7	3.448	242.0	5.9	2.97	0.13	-1.71	-1.67	2	
6961	0.21	0.74	21.5	3.625	230.9	0.1	5.05	0.06	-0.67	-0.99	2	3

Notes to TABLE 3b.

1. Average of photometry from ROA and Norris & Bessell (1975,1977). 2. Unable to verify star with periscope. 3. V photometry estimated from Schmidt V_R data differs from ROA V photometry by 0.2-0.3 magnitudes. 4. Average of photometry from ROA and Hawarden & Epps Bingham (1987). 5. Average of photometry from ROA, Hawarden & Epps Bingham (1987), and Martin (1981). 6. Crowded field. 7. Average of photometry from ROA, Cannon & Stobie (1973), and Norris & Bessell (1975, 1977).

TABLE 4. ω Cen Velocity Non-Members

ROA	V	$B - V$	$\log_{10}(\text{Int})$ (e $^-$)	v_r (km s $^{-1}$)	$\sigma(v_r)$ (km s $^{-1}$)	W(Ca) (\AA)	$\sigma(\text{W}(\text{Ca}))$ (\AA)	N
0482	12.78	1.48	3.995	-10.1	1.7	5.77	0.06	2
1093	14.88	1.02	4.006	-12.4	1.6	4.98	0.16	2
1182	14.81	0.65	3.253	-9.3	2.8	4.46	0.05	2
1233 ^a	14.90	0.67	3.921	-10.3	2.1	4.87	0.30	4
1263	14.81	1.05	3.457	-33.8	0.8	5.29	0.18	2
1304	15.16	0.56	3.643	-37.1	2.4	4.16	0.08	2
1386	15.25	0.82	3.357	21.2	1.1	5.37	...	2
1393	14.86	0.90	3.012	-16.2	2.3	5.16	0.57	2
1443	15.20	0.66	3.176	-46.7	1.3	4.95	0.06	2
1571	14.82	0.70	3.424	-69.2	5.4	4.86	...	2
1618	15.27	0.94	3.683	5.4	3.5	4.94	0.20	2
1773	14.87	0.92	3.346	3.2	4.2	5.21	0.17	2
1865	15.10	1.12	3.972	-29.6	2.8	5.16	0.21	4
1903	15.26	0.89	3.298	11.4	3.5	4.72	0.01	2
2205	14.84	0.83	3.102	9.6	2.3	4.70	0.20	2
2230	15.24	1.10	3.593	-13.3	4.2	5.05	0.17	2
2586	14.94	0.80	3.502	38.3	5.3	4.73	0.12	2
2592	14.94	1.10	3.120	-47.2	0.9	4.73	0.33	2
3316	14.82	0.94	3.569	25.4	1.9	5.04	0.08	2
3391	14.85	0.74	3.037	-22.8	10.8	4.98	0.01	2
4140	15.27	0.70	3.632	16.7	0.1	4.53	0.32	2
4674	15.01	0.99	3.485	43.1	4.5	4.99	0.08	2
5627	15.20	0.75	3.569	-12.3	1.8	4.66	0.32	2
5693	14.80	0.76	3.481	-30.0	5.0	4.36	0.29	2
6083 ^b	15.25	1.06	3.150	320.2	7.8	2
6124 ^c	15.15	0.75	3.471	10.7	0.7	4.81	0.22	2
6146	15.20	1.15	3.727	-8.4	0.5	5.02	0.00	2
6176 ^c	15.08	0.62	3.243	16.3	6.1	3.80	0.28	2
6267	14.83	0.74	3.337	32.5	4.9	5.22	0.08	2
6340	14.98	0.64	3.223	28.2	2.2	4.05	0.91	2
6397	15.15	0.56	3.367	-14.1	7.6	4.21	0.29	2
6577	14.98	0.87	3.625	60.4	0.8	4.64	0.24	2
6691	15.28	0.69	3.641	-10.3	5.5	3.13	0.05	2
6742 ^b	15.17	0.91	3.235	59.5	3.6	5.03	0.12	2
6875	15.10	0.98	3.667	-2.0	5.4	5.20	0.04	2
6886	15.20	0.58	3.418	3.0	7.6	3.75	0.04	2

^aUnable to verify star with periscope.

^b V photometry estimated from CCD 6840/95 data differs from ROA V photometry by 0.2-0.3 magnitudes.

^cConfused field. Possibly wrong star observed.

TABLE 5. Velocity Comparisons

Cluster	$\Delta(v_r)$ (km s ⁻¹)	σ (km s ⁻¹)	N
NGC 104	-0.4	1.5	17
NGC 6121	1.0	2.0	16
NGC 3201	0.3	1.5	36
NGC 6397	-1.5	1.9	9

TABLE 6. Median Values for the Error in a Single Observation

$\log_{10}(\text{Int})$ (e ⁻)	$\sigma(\text{W}(\text{Ca}))$ (Å)	$\sigma(v_r)$ (km s ⁻¹)	N
2.85	0.51	6.0	45
3.13	0.25	4.2	50
3.44	0.18	3.4	79
3.62	0.13	2.6	145
3.90	0.08	1.6	73
4.14	0.05	1.0	82
4.38	0.05	0.9	105
4.68	0.04	0.7	72
5.0	0.03	0.6	72

TABLE 7. Metallicity Averages for ω Cen

Sample	$\langle[\text{Fe}/\text{H}]\rangle$	σ	med($[\text{Fe}/\text{H}]$)	N
NDC scale				
SG	-1.59	0.19	-1.65	199
BG	-1.54	0.25	-1.63	144
BG ^a	-1.56	0.24	-1.65	163
GC scale				
SG	-1.61	0.25	-1.69	199
BG	-1.54	0.35	-1.66	144
BG ^a	-1.56	0.35	-1.68	163

^aOnly stars with $R > 8'$

The Abundance Spread Among Giants and Subgiants in the Globular Cluster ω Centauri

Nicholas B. Suntzeff

Dominion Astrophysical Observatory
Herzberg Institute of Astrophysics, National Research Council
5071 W. Saanich Road, Victoria, B.C. V8X 4M6, Canada

and

Cerro Tololo Inter-American Observatory
National Optical Astronomy Observatories¹
Casilla 603, La Serena, Chile
Electronic mail: nsuntzeff@noao.edu

Robert P. Kraft

University of California Observatories/Lick Observatory
Board of Studies in Astronomy and Astrophysics, University of California
Santa Cruz, California 95064
Electronic mail: kraft@ucolick.org

ABSTRACT

We present spectroscopic abundances and radial velocities for giant stars in the Galactic globular cluster ω Centauri based on the Ca II infrared triplet. Two samples of stars were observed: 234 stars at $M_V \sim 1.25$ on the lower giant branch at radial distances between $8'$ and $23'$, and 145 stars at $M_V \sim -1.3$ at radial distances between $3'$ and $22'$. We found 199 and 144 radial velocity members, respectively, in the two samples. These samples were corrected for evolutionary effects to provide an unbiased distribution of the underlying stellar metallicity. We find $\langle v_r \rangle = 234.7 \pm 1.3$, $\sigma_{obs} = 11.3$ km s⁻¹ (bright sample), and $\langle v_r \rangle = 232.9 \pm 1.2$, $\sigma_{obs} = 10.6$ km s⁻¹ (faint sample). The statistical errors of the dispersions are less than 1 km s⁻¹.

Previous metallicity studies found a non-gaussian metallicity distribution containing a tail of metal-rich stars. We confirm these results except our unbiased cluster metallicity distributions are narrower. They contain the following key features: (1) No very metal-poor stars (2) a sudden rise in the metal-poor distribution to a modal [Fe/H] value of -1.70 consistent with an homogeneous metallicity unresolved at the 0.07 dex level, (3) a tail to higher metallicities with more stars than predicted by simple chemical evolution models, and (4) a weak correlation between metallicity

¹ The National Optical Astronomy Observatories are operated by the Association of Universities for Research in Astronomy, Inc., under cooperative agreement with the National Science Foundation.

and radius such that the most metal-rich stars are concentrated to the cluster core. The unresolved metal-weak tail implies that the gas out of which ω Cen formed was well-mixed up to the modal metallicity of the cluster. Therefore, ω Cen like other Galactic globular clusters, seems to have formed in a pre-enriched and homogenized (up to the modal metallicity) environment.

The existence of a weak metallicity gradient supports the idea that ω Cen self-enriched, with the enriched gas sinking to the cluster center due to gas dissipation processes. We also note, however, that the metal-rich stars are more massive than the bulk of the stars in the cluster, and could also have sunk to the center by dynamical mass segregation over the lifetime of the cluster.

1. Introduction

ω Centauri is brightest globular cluster in the Milky Way Galaxy and one of the most unusual. It is the most massive cluster at $7 \times 10^6 M_{\odot}$ (Richer et al. 1991). It has a very large spatial extent on the sky with a core radius of $2.6'$ and a tidal radius of $45'$ (Trager et al. 1995). It is also one of the dynamically *youngest* clusters with a King concentration class of $c = 1.24$ (Trager et al. 1995) and a half-mass relaxation time of 5-10 Gyr (Binney & Tremane 1987 with data from Webbink 1985). Perhaps the most intensely studied peculiarity of ω Cen is the substantial spread in Fe-peak metallicity, with a range of approximately 1 dex. In the early photometric studies, Cannon & Stobie (1973) showed that the color-magnitude (c-m) diagram of ω Cen had an unusually wide giant branch, indicative of a heavy element abundance spread (cf. Norris & Bessell 1975), and Butler et al. (1978) found an abundance range of $[\text{Fe}/\text{H}] \sim -0.6$ to -2.2 from a ΔS -study of nearly half the cluster RR Lyraes. A similar range of metallicity was found from the spread in the $(V - K)_0$ vs. K_0 diagram for 82 ω Cen giants (Persson et al. 1980).

High resolution spectroscopic studies of ω Cen giants, starting with the pioneering work of Cohen (1981) and continuing to the present time (Mallia & Pagel 1981, Gratton 1982, Francois et al. 1987, Paltoglou & Norris 1989, Brown & Wallerstein 1993) confirmed the existence of a wide spread in $[\text{Fe}/\text{H}]$, and in addition indicated that the detailed [element/Fe]-ratios are often not those expected when one compares ω Cen giants with those found in mono-metallic clusters. This in turn suggests that the nucleosynthetic history of ω Cen is somehow different from that of other galactic globular clusters. Details concerning these differences and what they imply about the unique chemical evolution of ω Cen are the topics of several recent studies (Norris & Smith 1983, Paltoglou & Norris 1989, Brown & Wallerstein 1993), and especially a high resolution analysis of 40 ω Cen giants by Norris & Da Costa (1995).

Compared with these high resolution surveys, the present study has a more limited objective, *viz.*, that of determining an unbiased measure of the Fe-peak abundance spread in ω Cen. We attempt to derive the shape of the $[\text{Fe}/\text{H}]$ -distribution function using a complete sample of giants, drawn from a well-chosen, but limited interval of absolute magnitude. We describe this sample

(actually two samples) in more detail in Section 2. We note here that previous investigators have chosen their stars so as to be representative of the entire range of metallicities, and have not attempted to construct a distribution function based on an unbiased sample. We hope to recover here the shape of the distribution function, so that it may be compared with simple evolutionary models such as the classical “one-zone” model of chemical evolution (e.g., Searle & Sargent 1972, Hartwick 1976).

2. Sample Selection; Abundance Method

Our abundance procedure follows the technique developed by Olszewski et al. (1991), Armandroff & Da Costa (1991), Armandroff et al. (1992), Da Costa et al. (1992) and Suntzeff et al. (1992, 1993). We defer a discussion of specific observational details to Section 3, but describe the principles of the method as follows. In spectra of ω Cen and certain other mono-metallic cluster giants, we measure the pseudo-equivalent widths of the two strongest Ca II near-infrared triplet lines, $\lambda\lambda$ 8542Å and 8662Å. We define a quantity $W(Ca) = W(8542) + W(8662)$ which is plotted as a function of $(V - V_{HB})$, where V is the observed stellar visual magnitude and V_{HB} is the mean magnitude of the cluster horizontal branch (HB). The method depends on the well-known fact that in a V vs $(B - V)$ c-m diagram, giant branches become progressively taller (and bluer) with decreasing $[\text{Fe}/\text{H}]$. For any mono-metallic cluster of a given $[\text{Fe}/\text{H}]$, it turns out that the curve relating $W(Ca)$ to $(V - V_{HB})$ is a straight line with slope that is independent of $[\text{Fe}/\text{H}]$ and equal to 0.62 for stars lying above the HB, ie., with $(V - V_{HB}) < 0.00$ (see e.g., Figure 5 of Suntzeff et al. (1993); hereafter S93). Interpolation of the ω Cen giants within the grid of such straight lines for differing values of $[\text{Fe}/\text{H}]$ leads directly to an estimate of metallicity. The method has the obvious advantage that it is independent of interstellar reddening and (often somewhat) imprecise measurements of cluster distance moduli.

However, it is well known that the giant branch (GB) above the HB is bimodal: most of these stars are ascending for the first time to the red giant tip toward the He core flash, but about 20% belong to the post-HB stage of evolution, the so-called asymptotic giant branch (AGB) (Gingold 1974). Generally these stars are brighter than their first giant branch counterparts and the method described above will for these stars yield up $[\text{Fe}/\text{H}]$ -values that are somewhat too low. This presents a small problem in the analysis of stellar systems lying at large distances (e.g., dwarf spheroidal satellites of the Milky Way) in which only the brightest giants can be studied spectroscopically. This is not necessarily a limitation, however, in the study of the generally much nearer Galactic globular clusters.

Thus we have recalibrated the method using *subgiants*, i.e., cluster stars lying *below* the level of the HB in the c-m array. These stars are all on their first ascent up the GB. That the method works empirically for these subgiant stars will be demonstrated in Section 4; suffice it to say here that for subgiants, the slope of the lines relating $W(\text{Ca})$ to $(V - V_{HB})$ is different from that associated with the GB stars above the HB, and thus the method had to be recalibrated from

scratch. However, as a check on the results based on subgiants, we also analyzed a sample of ω Cen giants drawn from the tip of the GB.

The subgiant sample has a number of other advantages. The high density of stars in a very limited magnitude and color range will reduce the effects of systematic errors in converting line strength to the metallicity. Also, the subgiant stars are hot enough to be free of TiO formation, which can severely affect the measurement of metallicity in the Ca II region (S93).

We selected ω Cen giant star candidates from the tables of BV photometry published by Woolley (1966) (hereafter ROA). As noted above, two groups of stars were selected: a “subgiant sample” (SG sample) with $14.8 < V < 15.3$, and a “bright giant sample” (BG sample) with $12.2 < V < 12.8$. Different selection criteria were applied to the two samples.

The SG sample, with a mean $M_V \sim +1.25$, was drawn so as to avoid selection effects that would bias the resulting metallicity distribution. The magnitude limits were set by two competing constraints. The fainter limit was set both by the need to get a large sample in the small amount of observing time allocated to the project and by the photometric accuracy of the source. Cannon & Stobie (1973) (see also Section 3.2) found that the ROA photometry is well-calibrated (up to a simple zero-point shift in the B and V scales) with respect to their photoelectric photometry down to $V \sim 15.5$, but requires non-linear corrections below that level. The brighter limit was set by the need to avoid the region on the GB where the stars slow their evolution as they burn through the molecular weight discontinuity left from main sequence hydrogen burning (Fusi Pecci et al. 1990). They found from analysis of 13 cluster c-m diagrams, that the “bump” in the luminosity function is brighter than the HB by about 0.45 mag at $[\text{Fe}/\text{H}] = -2$ and fainter than the HB by about 0.3 mag at $[\text{Fe}/\text{H}] = -1$. With a mean HB magnitude of $V \sim 14.5$, this sets the upper limit at about 14.8 in V . We also made a cut in color at $(B - V) = 0.55$ to separate the GB from the region of the HB. In ω Cen, there are almost no stars at this color, so this provides a clean separation of the two evolutionary states.

To limit the number of field stars in the SG sample, we chose only stars from the ROA study that were considered as zero-proper motion members (i.e., proper motions of less than 100 in units given in the ROA work). We also excluded stars which had no proper motions. In almost all cases, these stars were within a cluster radius of $7.6'$: this effectively defines our inner radial limit for the sample. We excluded all stars with photometry listed as uncertain in ROA (9% of the sample). The stars with uncertain photometry had the same radial distribution as the rest of the sample and their exclusion should not bias the sample. Finally, we removed all stars that had any companion (in the ROA lists) that was nearer than $5''$ of a given star; such a companion would probably have contaminated the spectrum. A given star of magnitude V was excluded if there was any star within 5 arcsec that was brighter than magnitude $V + 1.0$. This reduced the list by only 3%. The final list contained 250 stars, which is essentially an unbiased sample of probable members between $8'$ and $23'$ from the cluster center. Note that this is a radial region well outside the cluster half-light radius of $4.8'$ (Trager et al. 1995).

The BG sample was created to tie into the previous abundance (both spectral and photometric) studies, and to include a sample of stars that lie mostly at smaller projected radii than the SG sample. We chose stars from the ROA lists lying outside a radius of $3'$, and which were subject to the following restrictions: proper motion less than 127 (in ROA units) or *no* measured proper motion; and stars with photometry not listed as “uncertain”. As with the SG sample, there was no red cutoff. The final list contained 190 stars. In addition to this sample, we also observed a list of ~ 20 bright giants, observed as nightly standards by Dr. Pat Seitzer as part of his program to measure the kinematics of the ω Cen cluster. Observation of these stars also permitted us to tie our abundance scale to that determined by previous investigators, particularly the recent high resolution studies of Paltoglou & Norris (1989), Brown & Wallerstein (1993) and Norris & Da Costa (1995). The Seitzer stars all have ROA numbers less than 233.

Both the SG and BG samples should be reasonably unbiased samples of the giants in the corresponding radial annuli. They are not quite complete samples however, because we have both excluded stars with poor photometry and adopted a conservative cutoff in proper motion that may exclude some bona fide members.

A c-m diagram showing the location of the two GB samples is shown in Figure 1.

To set up the abundance calibration of the Ca II triplet lines, we observed giants with luminosities comparable to those of our two ω Cen samples in the globular clusters listed in Table 1. The V_{HB} values and reddenings were mostly taken from Armandroff (1989). The value of V_{HB} for NGC 3201 which was taken from Brewer et al. (1993). The values of $V_{HB} = 14.54$ and $E(B - V) = 0.11$ were taken from Butler et al (1978) which are essentially identical to the independent work of Dickens & Saunders (1965). We note here that the cluster [Fe/H] abundances are based on the Zinn & West (1984) scale. We discuss possible changes in this scale later.

3. Observations and Data Reduction

3.1. Observational Techniques

We observed these samples of stars with the CTIO 4m telescope and the Argus multi-fiber system over a three-night period (24-26 Feb 1994 UT). On the first night, we observed for only 2.5 hours; the next two nights were reasonably clear. Our observing and data reduction procedures are fully described in S93, and we will not repeat them here. To briefly summarize, the Argus system allows 24 objects to be observed simultaneously over a $50'$ region of the 4m telescope prime focus field. Twenty-four exposures of the sky are also obtained with fibers set in close proximity to each stellar object. The reduced spectra covered the wavelength range $\lambda\lambda 8200 - 8800\text{\AA}$ with 1.2\AA pixel $^{-1}$ and 2.3 pixel resolution ($R = 3100$). A few small differences in our reduction technique compared with that of S93 should be recorded. First, because the stars in the present study are much brighter than those dealt with by S93, we created a single median sky spectrum per frame

for each group of 24 object spectra. Second, we applied only a single set of nightly wavelength solutions to all 48 fibers, based on exposures of a neon lamp which illuminated the dome white spot. The resulting spectra are thus on a reasonably good relative wavelength scale, but could suffer small shifts owing to slow nightly changes in the bench-mounted spectrograph (these shifts are taken out, as described in the next subsections). Each program field was observed twice with the same exposure times. All exposures of a given field were followed by exposures of a comparison source taken at the same telescope position. Multiple exposures were co-added for measurement of the velocities and equivalent widths. The individual exposures, however, were saved to allow one to make an estimate of the errors.

The observed standard stars are listed in Table 2, and the observed program stars are listed in Table 3a (BG sample) and 3b (SG sample). Table 4 contains the observed stars in the BG and SG samples that turned out to be non-members based on the radial velocities. The Tables 2 and 3 contain the stars names, $(V - V_{HB})$ magnitudes, and dereddened $(B - V)_0$. We list the average intensity in the co-added spectra in units of $\log_{10}(e^-)$ where “e-” refers to a detected photo-electron. Table 3 also lists the radial distance (in arcminutes) from the cluster center. We observed 145 stars in the BG sample, 234 in the SG sample, and 17 brighter giants for overlap with the Seitzer radial velocity work. The number of observed stars is somewhat less than the full sample due to fiber positioning limitations.

3.2. Photometry of the sample

In order to measure the stellar metallicities based on the Ca II triplet lines, we need V photometry of only modest accuracy. An error of 0.1 mag in V will introduce an error of only 0.02 dex in $[\text{Fe}/\text{H}]$ for a metal-poor star. We have constructed average magnitudes from many sources in the literature. For the BG sample, we have used the magnitudes listed in the ROA study, Eggen (1972), Cannon & Stobie (1973), and Lloyd Evans (1983a) as the primary sources, and Bessell & Norris (1976), Hesser, et al. (1977), Hawarden & Epps Bingham (1987), Martin (1981), and Alcaïno & Liller (1984) as secondary sources. There are well-known shifts between the various tables of photometry. We have calculated simple zero-point shifts of the primary photometry lists to the system of Cannon & Stobie (1973) as follows: ROA (0.06,-0.07); Lloyd Evans 1983a (-0.03,0.00), Eggen 1972 (-0.06,0.03) where the numbers refer to the additive constants applied to $(V, B - V)$ in those lists. There was not enough overlap among the secondary sources, so these were used as given. The averaged photometry from all the sources is listed in Table 3a. Many of the bright giants show large variations in V as noted in Table 3a.

We checked the ROA V photometry for radial-dependent differences with the photoelectric photometry. Other than the zero-points listed above, there was no significant non-zero gradient from 5 to 21' for the 135 non-variable red stars in common. However, the photometry of stars from 4 to 5 arcminutes from the Lloyd Evans (1983a) work was ~ 0.2 mag *fainter* than the ROA magnitudes. Whether the ROA or the Lloyd Evans (1983a) photometry is in error is difficult to

say, but the V magnitudes within 5 arcminutes of the cluster center may be suspect.

To compare with the SG sample, there are 138 fainter stars with published photoelectric (pe) photometry listed in Hawarden & Epps Bingham (1987), Cannon & Stobie (1973), Martin (1981), and Norris & Bessell (1975, 1977). If we restrict the comparison to red stars with $B - V > 0.6$ and $13.1 < V < 15.3$, the median differences are 0.04 mag or less in V and 0.04 in $B - V$ between the ROA and the other lists with dispersions (clipped at 3-sigma) of 0.07 mag or less. There was no non-zero gradient in the difference between the V magnitudes from the ROA and pe photometry as a function of cluster radius from $10'$ to $23'$. We use the ROA photometry for the SG sample averaged with the photometry from the other lists. The adopted photometry is listed in Table 3b.

The photometry of the SG sample was checked with CCD data obtained on the CTIO Curtis Schmidt telescope. A four frame mosaic of ω Cen in red and blue colors was obtained with the Thomson 1024x1024 CCD (1.86 arcsec pix^{-1}). The red data, taken with a 6840/95 filter, were analyzed with the photometric packages DAOPHOT and ALLSTAR (Stetson 1994). The frames were star subtracted, and then only the stars in the SG sample were added back in. These frames were then measured with the DAOPHOT aperture photometry program with a digital aperture of $7.5''$ radius. We calculated a simple linear transformation between these red instrumental magnitudes and the corrected ROA V magnitudes for the SG sample. For 108 stars in overlap regions, the average estimated (statistical) error in a single magnitude is 0.03 mag. The transformation between red instrumental magnitude and V had a dispersion of 0.07 mag, which is the same as the quoted accuracy of the ROA V magnitudes for single plate measurements.

The transformed red magnitudes (which we will call V_R) are an approximation to the true V magnitude, since $[\text{Fe}/\text{H}]$ would be expected to affect V differently than a redder color. In Table 3b, we flag the four stars where the ROA V values differ by 0.2-0.3 mag from the V_R CCD photometry. No stars differed by more than 0.3 magnitude. In the SG sample, the two estimates of the V magnitude agree to within 0.10 mag for 83% of the stars, and 94% of the stars agree to within 0.15 magnitude.

There was a small gradient in $\Delta(V)(\text{CCD-ROA})$ of -0.012 mag arcmin^{-1} from 8 to $17'$ radius and 0 -0.012 mag arcmin^{-1} out to $24'$. Evidently with the higher quality CCD magnitudes a small non-zero gradient is evident in the ROA data, but the total effect of the gradient of ~ 0.1 mag will not affect the abundance results and we ignore it.

We have also used the CCD frames to locate all the stars in the SG sample which were observed. The CCD xy positions were transformed to the ROA astrometric positions with an accuracy of 0.4 arcseconds rms (root-mean-square). At the telescope, we noted a few cases where there was some ambiguity as to which star to assign to the fiber. We used the CCD frames (after the run) to verify that the correct stars were indeed observed. Only two stars were found to be incorrect. ROA 6124 was not found at the telescope, yet it appears at the correct position in the CCD frames. Presumably, the fiber positioner lost its absolute location for this star. Star ROA 6176 was not located at the telescope nor on the CCD frame.

3.3. Measurements of Radial velocities and Ca II Triplet Equivalent Widths

The Ca II triplet equivalent widths ($W(\text{Ca})$) and radial velocities were measured in the same manner as in S93, with a few differences noted below. These values for the program and standard stars are listed in Tables 2, 3, and 4. The co-added spectra were used to measure the values given in the tables, while the individual spectra were used to calculate a standard deviation in the mean. This standard deviation, which is listed as σ in the tables, crudely represents the measurement error in a single spectrum that was used in the co-addition to the final spectrum. Also listed in the tables are the number of independent observations.

The standard clusters give the same $W(\text{Ca})$ as published in S93. We find the following differences in the sense of (this work - S93): 47 Tuc, (0.12Å, 0.16Å, 11); M4, (0.07Å, 0.12Å, 18); and NGC 6397 (-0.03Å, 0.09Å, 20), where we list the mean difference, standard deviation, and number of stars. The higher dispersion in the 47 Tuc stars is probably due to variability of stars on the RGB.

We reduced the radial velocities slightly differently from S93. A single nightly wavelength calibration was used to correct all spectra to an approximate linear wavelength scale. All stellar spectra were cross-correlated with respect to three velocity templates (47 Tuc stars) exactly as in S93. Fiber-to-fiber “velocity” differences were calculated by cross-correlating the nightly twilight spectra with an averaged twilight spectrum, and these offsets were subtracted from the stellar velocity in a given fiber. At this point, all the velocities from spectra on a given frame are on a relative velocity system. To bring all the frames onto a relative velocity system, we calculated frame-to-frame offsets by cross-correlating the sky spectrum (averaged over all 24 sky fibers) and subtracted this offset from all the velocities in a given frame. The same shifts were applied to the comparison lamp arcs which were observed after the sequence of observations in every field. The final adjustment was made by comparing the observed velocities with the following published velocities: 47 Tuc, Mayor et al. (1983); M4, Peterson et al. (1995); and NGC 3201 Côte et al (1994).

On all three nights, a single field of bright giants (provided by Pat Seitzer) was observed. The average velocity differences for the 24 stars were: night1 - night2, (+0.5 1.2), and night1-night3 (+0.3,1.3) where we have listed the mean difference and standard deviation of the mean in units of km s^{-1} . For a field that was observed in 47 Tuc on nights 2 and 3, we find (-0.2, 1.9) km s^{-1} . Evidently the relative velocity zero point is accurate to better than 1 km s^{-1} for the three nights. The cross-correlation of the comparison lamps yields an independent test of the relative velocity zero points. The 24 spectra in the object fibers were co-added and cross-correlated. The rms difference between the co-added comparison spectra and a template was 0.5 km s^{-1} , consistent with a relative velocity zero point accurate to better than 1 km s^{-1} .

In Table 5, we compare the velocities in Table 2 with the published values listed above. In addition, we compare the NGC 6397 velocities with the values in S93. The comparison shows that for bright stars, the individual velocities are accurate to 2 km s^{-1} or better which we adopt as the

minimum error in the individual velocities. The rms differences for the 4 cluster velocities given in Table 5 imply an absolute velocity zero point error of about 1 km s^{-1} .

Individual velocities for ω Cen stars have not been published, but mean properties have been given by Meylan & Mayor (1986) as summarized by Pryor & Meylan (1993) where they quote $\langle v_r \rangle = 232.2 \pm 0.7$ and $\sigma_{obs} = 12.20 \pm 0.50 \text{ km s}^{-1}$ for 318 stars in an annulus between $0.3'$ and $23.4'$. For the obvious cluster members in our two samples, we find $\langle v_r \rangle = 234.7 \pm 1.3$, $\sigma_{obs} = 11.3 \text{ km s}^{-1}$, $N = 161$ for the BG+Seitzer sample, and $\langle v_r \rangle = 232.9 \pm 1.2$, $\sigma_{obs} = 10.6 \text{ km s}^{-1}$, $N = 199$ for the SG sample. We have added the absolute velocity zero point error of 1 km s^{-1} to the statistical mean errors to derive the quoted errors in the mean.

Excluding all stars with $\sigma(v_r) > 8 \text{ km s}^{-1}$ in the SG sample does not change these numbers significantly. The statistical errors on the dispersions ($\sigma_{obs}(2N)^{-0.5}$) are all less than 1 km s^{-1} . The slightly smaller velocity dispersions in our samples are probably due to the falloff of dispersion with radius and the somewhat larger mean radius of our samples.

The large radial velocity of ω Cen allows a clean separation between members and non-members. All stars at greater than $3\sigma_{obs}$ from the cluster mean were considered non-members and are listed in Table 4. In Figure 2, we show the c-m diagram for all the members and non-members observed in ω Cen. Not surprisingly most non-members lie well off the giant branch.

3.4. Estimated Errors in W(Ca) and v_r

The values for σ given in Tables 2 and 3 are estimators for the errors in the derived quantities. The mean errors are formally $\sigma/(N)^{1/2}$ but since N is typically 2, an individual mean error is not well determined. A more robust way to estimate the errors is to correlate the errors with the mean intensity and use the latter to estimate the error. In Figure 3 we plot all the σ values for N=2 in our data set as a function of the mean intensity in the co-added spectra. We also plot curves which represent the median values of σ from this and other Argus data in our archives. These ensemble median values are given in Table 6. A simple Monte Carlo calculation shows that for a normal distribution sampled twice, $\langle \sigma \rangle = 0.79$ and $\text{med}(\sigma) = 0.67$ where σ is the dispersion calculated for two points. Therefore, the mean error of a measurement based on the co-added spectrum should be $\text{med}(\sigma)/(0.67 \times \sqrt{2})$ which is roughly the $\text{med}(\sigma)$ given in Table 6. The mean intensity is not a perfect indicator of the errors because the stars with truly large values of σ in Tables 2 and 3 do have poorly determined velocities and equivalent widths.

As a compromise, we suggest the following estimator for the errors: the error in a quantity is the larger of two values, $\text{med}(\sigma)$ and $\sigma/(2)^{1/2}$ for N=2. For the two samples in ω Cen, the median errors in W(Ca) are 0.05 and 0.16\AA .

4. Calibration and Results

4.1. The Reduced Equivalent Widths for the Two Samples

Except in the case of 47 Tuc, two groups of stars were observed to mimic the luminosity range of the ω Cen samples. The block of observing time allocated to the project proved inadequate to permit the acquisition of a 47 Tuc sample analogous to the ω Cen SG sample; the effect of this on our results should be slight, and is discussed a little later.

In Figure 4, we plot $W(Ca)$ as a function of $(V - V_{HB})$ for the calibrating clusters. The long straight solid lines are the best fit ridge lines with constant slope of 0.62 transferred from Figure 5 of S93 for the clusters M71, M4 and NGC 6397. The dashed line is the fit to the NGC 3201 data from this paper with the same slope. The solid and dashed lines, all having a slope of 0.62 in this diagram, correspond to the stars of the BG sample of each of the calibrating clusters. The dotted straight lines, on the other hand, are “by eye” fits to the sample of SG stars of Table 2. Note that the slopes of the dotted lines are essentially the same (0.35), but differ from the slope associated with the bright star samples. As noted above, we did not observe SG stars in 47 Tuc, but assumed by analogy with the situation for the BG sample, that the 47 Tuc SG stars would fall along a line of slope 0.35 in a position homeomorphic to the location of the lines representing the other clusters.

For the BG sample, if we form the “reduced” equivalent widths of the two strongest Ca II lines as $W' = W(Ca) + 0.62((V - V_{HB}))$, the parameter W' becomes an estimator of $[Fe/H]$, as previously shown in S93, Armandroff et al. (1992), and Armandroff & Da Costa (1991). The averaged values of W' and the errors in the mean for the standard clusters based on the BG sample are given in Table 1. The $\langle W' \rangle$ values for 47 Tuc, M4, and NGC 6397 in Table 1 are essentially identical to the values for these clusters listed in S93 of 4.75, 4.08, and 2.30Å.

In analogy with the BG sample, we can also form a reduced equivalent width for the SG sample, but with a different slope. If we force this reduced equivalent width to be on the same scale as that of the brighter giants, we find $W' = W(Ca) + 0.35((V - V_{HB})) - 0.19$. For the subgiant stars in M4, NGC 3201, and NGC 6397, we find the following values of $\langle W' \rangle$ for the SG sample: $4.11 \pm 0.02\text{Å}$, $3.54 \pm 0.04\text{Å}$, $2.36 \pm 0.03\text{Å}$, which are essentially identical to the mean values in Table 1. We can treat the W' system for both the BG and SG samples as the same.

In Figure 5 we plot the $W(Ca)$ values for the ω Cen giants in the two samples. The distribution of stars with respect to the ridge lines is very similar in the two samples, and we can expect that both samples will give very similar metallicity distributions. There is a sharp cutoff at low metallicity which is parallel to the ridge lines and most of the stars in the sample are near this cutoff. There is also a less populated tail up to line strengths significantly greater than that of 47 Tuc giants. The fact that there is no similar tail or even a single star at lower metallicities (in the SG sample) strongly indicates that ω Cen did not form in situ with lower metallicity gas, but instead, formed in the presence of mono-metallic gas as did almost all the other galactic globular

clusters. The four stars in the BG sample that evidently have low metallicities may well be AGB stars, which lie too bright with respect to RGB stars at the same $B - V$ colors.

4.2. The Metallicity Calibration

We have two available calibrations to convert W' into $[\text{Fe}/\text{H}]$. The first calibration is from S93 where we plot $[\text{Fe}/\text{H}]$ as a function of $\langle W' \rangle$ for galactic globular clusters. We show this relationship in Figure 6. We have drawn two line segments by eye to mimic the mean relationship. These relationships are:

$$\begin{aligned} [\text{Fe}/\text{H}] &= 0.37W' - 2.79, \quad W' < 4.1\text{\AA} \text{ and} \\ [\text{Fe}/\text{H}] &= 0.73W' - 4.28, \quad W' > 4.1\text{\AA}. \end{aligned}$$

The calibration on the metal-poor end is slightly different than the one given in S93, because we have forced the calibration to be continuous at the break point, rather than use least squares for the two segments which produces a discontinuity at $W' = 4.1$.

For the second calibration, we can use the actual $[\text{Fe}/\text{H}]$ values of ω Cen giants from the high-dispersion work of Norris & Da Costa (1995) for the 24 stars in common. In Figure 7 we plot the relationship between individual W' values and the $[\text{Fe}/\text{H}]$ and $[\text{Ca}/\text{H}]$ for the stars in common. We have plotted both $[\text{Fe}/\text{H}]$ and $[\text{Ca}/\text{H}]$ to illustrate the following point. The W' value for a star is a function of T_{eff} , $\log(g)$, broadening parameters, $[\text{Ca}/\text{H}]$, and the continuous opacity. By plotting along isochronal sequences (as we do when we plot $W(\text{Ca})$ as a function of $(V - V_{HB})$) and taking out the mean trend, we have formed what appears to be a functional dependence of W' on a single value - $[\text{Fe}/\text{H}]$. This is valid insofar as $[\text{Ca}/\text{Fe}]$ is a monotonic function of $[\text{Fe}/\text{H}]$, and that $[\text{Ca}/\text{Fe}]$ has the same relationship in individual stars in ω Cen as the average trend seen in the globular clusters. The Norris & Da Costa (1995) work suggests that $[\text{Ca}/\text{Fe}]$ is a different function of $[\text{Fe}/\text{H}]$ than the average trend for globular clusters in that $[\text{Ca}/\text{Fe}]$ remains high even for metal-rich stars. If this is the case, the globular cluster calibration shown in Figure 6 will be wrong for metal-rich stars and it will *over-estimate* the true value of $[\text{Fe}/\text{H}]$ by up to 0.3-0.4 dex. In addition, the larger scatter seen in Figure 7 for the $(W', [\text{Fe}/\text{H}])$ compared to $(W', [\text{Ca}/\text{H}])$ may also indicate that there is real scatter in the $[\text{Ca}/\text{Fe}]$ relationship in ω Cen.

We have fit a functional form to the $(W', [\text{Fe}/\text{H}])$ relationship shown in Figure 7 as

$$[\text{Fe}/\text{H}] = -2.45\text{\AA} + 0.223W' + 0.0152(W')^2, \quad 2.6 < W' < 5.4\text{\AA}. \quad (1)$$

The two values of $[\text{Fe}/\text{H}]$ will be called $[\text{Fe}/\text{H}]_{ZW}$ and $[\text{Fe}/\text{H}]_{NDC}$. One final refinement will be made to the derived metallicities. In deriving $[\text{Fe}/\text{H}]$ we have used the quantity $(V - V_{HB})$. The level of the HB however, depends on $[\text{Fe}/\text{H}]$, so we must correct the quantity $(V - V_{HB})$ for $[\text{Fe}/\text{H}]$, and rederive the metallicity. To do this, we have adjusted V_{HB} as

$$V_{HB} = 14.54 + 0.20([\text{Fe}/\text{H}] + 1.7) \quad (2)$$

Here we have assigned the average value of V_{HB} based on the RR Lyraes to the metallicity of $[\text{Fe}/\text{H}]=-1.7$ (which is the modal value of $[\text{Fe}/\text{H}]$ in ω Cen), and assumed a slope of 0.20, which is a compromise value among the slopes of the $(M_V, [\text{Fe}/\text{H}])$ relationship of RR Lyraes (Sandage & Cacciari 1990). The values of V_{HB} for ω Cen adjusted in this manner have been used to recalculate $(V - V_{HB})$ and the values listed in Table 3 have been corrected for this effect. The final values of $[\text{Fe}/\text{H}]$ listed in Table 3 also reflect the adjustments in V_{HB} . The effect of this refinement is small and affects only the metal-rich stars: the adjustment makes the metal-rich star appear brighter with respect to V_{HB} , and as can be seen in Figure 4, this will make the star more metal-poor. The change is no larger than ~ 0.1 dex.

In Figure 8 we illustrate the change in the appearance of the IR Ca II triplet lines in three stars drawn from the SG sample. The equivalent widths of the triplet lines change by a factor of two in this illustration, which corresponds to a change of a factor of 10 in $[\text{Fe}/\text{H}]$.

We leave this section with a final comment on the metallicity scale. While we have no independent spectroscopic evidence to decide which scale is correct, the colors of the stars appear to support the $[\text{Fe}/\text{H}]_{NDC}$ scale. In Figure 9, we plot the derived $[\text{Fe}/\text{H}]$ values for the two scales as a function of dereddened $(B - V)$. The $(B - V)_0$ for a star in this evolutionary position should have essentially the same functional dependence on $[\text{Fe}/\text{H}]$ as $(B - V)_{0,g}$, which is the mean dereddened color of a globular cluster RGB at the level of the horizontal branch. Figure 9 shows that the $[\text{Fe}/\text{H}]_{NDC}$ scale reproduces the mean trend of $(B - V)_{0,g}$ for globular clusters better than the $[\text{Fe}/\text{H}]_{ZW}$ scale. The extremely high metallicities in the $[\text{Fe}/\text{H}]_{ZW}$ scale are not confirmed by very red colors.

5. The Metallicity Distribution Functions

5.1. Evolutionary Corrections to the Abundance Histogram

Before we can discuss the metallicity distribution function, we need to make one final correction to our samples. By choosing samples of stars via cuts at constant V , we will subtly bias our data due to the complex way in which stars evolve as a function of metallicity. There are three major effects.

The first effect is that stars of higher metallicity will have a larger bolometric luminosity at a fixed V . This is mainly due to the fact that the bolometric correction (to V) is only a weak function of $[\text{Fe}/\text{H}]$ at a given $(B - V)$ but is a strong function of $(B - V)$ for the range in temperatures and metallicities of the stars considered here. The metal-rich stars, which have redder colors, have a larger bolometric correction and are intrinsically more luminous at a given V . In this case, the higher metallicity stars will evolve more quickly through the cut in V and

therefore be underrepresented.

The second effect is for a given age of the underlying population, a higher metallicity star will have a higher mass. For instance, at $M_V = 1.25$ which is representative of the SG sample, the mass increases from 0.82 to $0.87M_\odot$ as the metallicity increases from $[\text{Fe}/\text{H}] = -1.78$ to -0.78 for 14 Gyr isochrones (Bergbusch & Vandenberg 1992). Since mass functions, defined as $dN = AM^{-x}d\log(M)$ typically have positive values of x (Richer et al. 1991), the metal-rich stars will again be underrepresented with respect to a fixed number of main sequence stars.

The third effect is due to mass segregation where more massive stars sink to the center of the cluster. We will come back to this point later. Other effects, such as variable mass functions (as a function of $[\text{Fe}/\text{H}]$) are further complications which will not be considered here.

The first two effects can be corrected for by numerical integration of theoretical luminosity functions, as given in Bergbusch & Vandenberg (1992). The second effect however, requires that we define a base population to which we will correct all the masses and this correction will require the adoption of a mass function. We cannot use the subgiant branch or main sequence turnoff as the base, since the number of stars per unit interval in these sequences are also a function of metallicity. We will use the brightest unevolved main sequence stars, with masses between 0.6 and $0.7M_\odot$ as the base. The choice of the brightest unevolved main sequence stars minimizes the effects of the adopted mass function. We calculate the correction factor to the raw histogram as the ratio of the number of stars between 0.6 and $0.7M_\odot$ to the number of stars in the given V interval. We will use an apparent distance modulus to the cluster of 13.83 . This was calculated using the $V_{HB}([\text{Fe}/\text{H}])$ relationship given above with a modal cluster metallicity of -1.7 .

The choice of the mass function is not clear. Richer et al. (1991), in their Figure 10, present mass functions for many clusters, including ω Cen. The four metal-poor clusters in that figure have rather flat mass functions from 0.7 to $0.4M_\odot$. A simple fit to these 4 clusters yields an average value of $x = 0.8 \pm 0.3$. However, the measured mass function at $0.8M_\odot$ in ω Cen is extremely steep ($x \sim 4$) until $0.6M_\odot$ where it flattens to $x = -1$. Dynamical processes can sink more massive stars to the cluster center, but given the distance of these ω Cen fields from the cluster center (5 and $9r_c$) and the long half-mass relaxation time of the cluster, this seems unlikely. It should be noted that the mass function at the high mass end is based on a very few number of stars, and we suspect that the problem lies with counting statistics. We will adopt a more typical mass function with $x = 1.0$.

We find that the correction factor is relatively independent for $[\text{Fe}/\text{H}] < -1.0$ but is much more dependent on the mass function at higher metallicities. For instance, the correction factor at $[\text{Fe}/\text{H}] = -0.65$ rises from 15% to 26% as the mass function power law increases from $x = 1$ to 2 . The correction factors are plotted in Figure 10.

In Figure 11 we present the metallicity histograms, corrected for the evolutionary effects, and in Table 7 we give the basic cluster statistics for ω Cen.

5.2. Comparison of the SG and BG samples

Both the cluster averages given in Table 7 and the histograms for the two samples shown in Figure 11 show that the two samples have very similar distributions. From smoothed histogram fits, we estimate the modal value as $[\text{Fe}/\text{H}]=-1.70$ for the two distributions. There is a sharp rise from lower metallicities to the modal value of the distribution, and a less steep decline to higher metallicities. A tail with a few stars extends to very high metallicities.

There are, however, small differences in the two sample distributions. If we pare the BG sample to only include stars at cluster radii greater than $8'$ to be consistent with the SG sample, we find that a two-sided Kolmogorov-Smirnov (K-S) test (Nemec & Harris 1987, Press, et al. 1992) gives a probability of the rejection of the hypothesis that the two samples are drawn from the same parent population at 80%, independent of which metallicity scale is chosen. The sense of the difference is that the BG sample has a small number of metal-rich stars that are much more metal-rich than the SG sample.

It is difficult to pinpoint the reason for the small differences in the distributions. The calibrations in Figures 6 and 7 cover the range in line strengths observed. One may suspect that because the conversion of $W(\text{Ca})$ to W' shown in Figure 4 does not extend to metallicities higher than those in M4 for the SG sample, the metal-rich end of the SG metallicity scale may be suspect. More calibration data will be needed to resolve this problem.

One may also suspect the calibration of the BG sample. There is a trend of increasing $W(\text{Ca})$ as a star ascends the RGB shown in Figure 4. But as shown by Erdelyi-Mendes & Barbuy (1991), for $[\text{Fe}/\text{H}]=-1$, there is almost *no* gravity effect on $W(\text{Ca})$ at $\log(g)=0$, while there is a trend of increasing line strength with decreasing T_{eff} . The trend seen in Figure 4 is due to mostly the change in T_{eff} on the RGB. According to Norris & Da Costa (1995), the metal-rich stars have unusual $[\alpha/\text{Fe}]$ ratios. As discussed by Vandenberg (1991), different abundances of the intermediate α -elements will affect the position of the isochrones in lower temperature stars. Thus, the use of the correction of $W(\text{Ca})$ as a function of $(V - V_{HB})$ which is based on normal globular cluster iso-abundance sequences may also be suspect. Isochrone models which decouple CNO, $[\alpha/\text{Fe}]$, and $[\text{Fe}/\text{H}]$ are needed to investigate this effect.

Since the difference between the two samples is really seen only in the few metal-rich stars, we must also be concerned that the line strengths, either in the high-dispersion data of Norris and Da Costa (1995) or this work, could be affected by molecular formation or non-LTE ionization effects. For instance, the α -element abundances tabulated in the Norris and Da Costa (1995) work rely on neutral lines which could be affected by non-LTE ionization effects in the cooler stars or errors in the T_{eff} calibration. New high S/N high-dispersion spectra of the metal-rich giants would be very useful in assessing these effects.

5.3. Metallicity gradient in ω Cen

In Figure 12 we plot the radial distribution of the metallicity in ω Cen. In a general sense, this diagram shows there is a large dispersion in metallicities at all radii, and there is no large gradient in the average metallicity as a function of cluster radius.

There are also some indications of possible trends buried within the large metallicity dispersion. There appear to be a few very metal-poor giants in the BG sample that are not seen in the SG sample. While these could be metal-poor giants, it is more likely they are AGB stars, which will have artificially low $W(\text{Ca})$ values due to their position in the c - m diagram (S93). We have flagged these stars (ROA 342,383,429,435) in Table 3a. We remove these stars from the following discussions.

There appears to be a trend in that the most metal-rich giants in the BG sample lie a small radii. This trend is not seen in the SG sample, but the SG sample does not probe the inner part of the cluster where most of these stars lie. If we cut the BG sample in two at a given $[\text{Fe}/\text{H}]$, we can compare the radial distributions with a K-S test. We find that if the cut is made in the range of $-1.1 < [\text{Fe}/\text{H}] < -1.3$, the two distributions are different at the 70% level. The effect disappears if cuts are taken at lower metallicities. Thus we have evidence, albeit weak, that there is a some segregation in metallicity as a function of radius.

According to Freeman (1985), giants lying beyond the limits of the ROA catalog have systematically weaker CN bands than the majority of stars inside the $r_t = 22$ arcmin radius. Weaker CN bands are believed to be an indication of reduced metallicity, although the size of the effect has not been calibrated. A comparison of CN band strengths in clusters such as M13 (at $[\text{Fe}/\text{H}] = -1.6$) with M92 (at $[\text{Fe}/\text{H}] = -2.2$) suggests that over this 0.6 dex decline in metallicity, CN bands essentially disappear (cf. Suntzeff 1981, Carbon et al. 1982). Thus over the metallicity range encountered among ω Cen giants we might expect that a change in $[\text{Fe}/\text{H}]$ as small as 0.3 dex could induce a significant change in the strength of the CN bands. However, other effects related to evolutionary state may also be at work (see review by Kraft 1994), and even among giants in the same evolutionary state and metallicity, but in different clusters, CN band strengths can differ (Langer et al. 1992). The interpretation of this effect and its influence on the abundance distribution derived here, although probably small, is not entirely clear.

5.4. Discussion

The metallicity histograms shown in Figure 11 verify the general shape of the metallicity histograms given by Butler et al. (1978), Norris (1980), Persson, et al. (1980), and Da Costa & Villumsen (1981): a sharp rise at a low metallicity and a tail of stars to higher metallicity, although our unbiased sample shows that there are relatively few stars on the metal-rich tail. Our data do not support the existence of a rather large population of very metal-poor stars found by

Butler, Dickens & Epps (1978) in their ΔS study of 58 RR Lyraes in ω Cen, where they found that one quarter of these stars had $[\text{Fe}/\text{H}] \lesssim -1.90$. The derived metallicities in their study, which were based on image-tube spectra, had rms errors of 0.4 dex and presumably the low-metallicity stars are the low-metallicity tail of the error distribution. A new study of the metallicities of RR Lyraes in ω Cen is called for, since CCD spectra can give abundances based on ΔS values good to 0.15 dex in $[\text{Fe}/\text{H}]$ (Suntzeff et al. 1994).

Is there a metal-poor tail? If we fit the SG distribution with a gaussian from the metal-poor tail up to the modal value of $[\text{Fe}/\text{H}] = -1.70$, we find a dispersion of 0.07 dex in $[\text{Fe}/\text{H}]$ for 69 stars. If we only take the 36 stars with $W(\text{Ca})$ errors less than median value of $\sigma(W(\text{Ca}))$ of 0.16\AA , we still find the same dispersion. Note that the relations above give $\sigma([\text{Fe}/\text{H}]) \approx 0.35\sigma(W(\text{Ca}))$ at the metal-poor end. The errors show that we are just at the limit of detecting a real metallicity spread on the metal-poor tail. We can conclude that the metal-poor tail of ω Cen stars is consistent with these stars having formed in a proto-cluster gas clouds with a metallicity spread of less than about 0.07 dex in $[\text{Fe}/\text{H}]$. This level of chemical homogeneity is typical for other globular clusters (Suntzeff 1993). Some clusters have limits of inhomogeneity half this value, but these clusters generally have had many fewer stars observed at much higher signal-to-noise. Better spectra (with multiple observations) could improve the estimate of the metal-poor tail homogeneity in ω Cen. It should be noted that we cannot use the BG sample for this because of the AGB contamination.

The overall metallicity distribution can be compared to a model of chemical evolution (Searle & Sargent 1972) as conveniently parametrized by Hartwick (1983) and Pagel (1992). Pagel describes this “Simple Model” as a “one-zone model treated in the instantaneous recycling approximation with constant yields for ‘primary’ nucleosynthesis products from short-lived massive stars...,” of the functional form:

$$\frac{ds}{d \ln z} \propto \frac{z}{y} e^{-(z-z_0)/y} \quad (3)$$

Here z is the instantaneous mass fraction of the metals, s is the mass of stars with abundances $\leq z$, y is the yield, and z_0 is the initial abundance of the gas. The distribution is 0 for $z > \ln(m/g)$ where g is the mass of gas and dust, and $m = g + s$ is the total mass of the system. We have modified this distribution following Zinn (1978) and Bond (1981) to include a non-zero starting metallicity. This distribution peaks at $z = y$ (provided that $z_0 < y$) which leads one to assume that the yield is very roughly the solar metallicity for simple models of disk evolution, which is verified from calculations of nucleosynthetic yields where $y \sim 0.01$ (Matteucci 1983).

The metallicity distribution for ω Cen stars peaks at a much lower metallicity ($z = 0.0003$) implying a much lower yield is needed. Low yields are calculated for metal-poor stars ($y \sim 0.001$; Matteucci 1983) but this is still not low enough. The yield can also be lowered by assuming very steep mass function on the main sequence or by introducing gas loss at a rate proportional to the star formation rate. This latter refinement by Hartwick (1978) is suggested by the simple idea that

the number of number of supernovae should be related directly to the star-formation rate. In this case, the distribution has the same functional form but the total mass m is no longer constant, and the yield is replaced by an effective yield which is a factor of $(1 + \Lambda)$ smaller than the actual yield, where Λ is the ratio of mass loss to star formation (in Pagel’s notation).

An example fit to the data using a Simple Model is shown in Figure 13. Here we have used an initial metallicity of $[\text{Fe}/\text{H}] = -1.78$, and an effective yield of 0.00012. We have convolved the model with the observed median error of 0.07 dex, and binned the model data for comparison. Larger effective yields will improve the fit to the metal-rich tail but will broaden the peak well past the observed limits. Smaller effective yields will narrow the model peak (and improve the fit in this Figure) but will produce even fewer metal-rich stars.

If the Simple Model is correct, then the poor fits as evidenced in Figure 13 can be explained in two ways. We can lower the yield (thus underproducing still further the metal-rich stars) and postulate a second generation of stars formed with a higher mean metallicity to account for the metal-rich tail. Pre-enriched gas falling back on the cluster after the initial star formation wave is a natural explanation for this. We can also increase the yield slightly to fit the metal-rich tail (which will broaden the metallicity peak), and postulate a homogeneous initial population of stars at $[\text{Fe}/\text{H}] \approx -1.7$. Both scenarios require two generations of stars.

If the low effective yields are interpreted as cluster mass loss, then $\Lambda > 10$ implying almost the whole cluster mass is lost (Zinn 1978). Smith (1984) discusses the fate of a proto-cluster in the presense of severe mass loss. If the mass loss is impulsive such that the cluster cannot adjust adiabatically, it will disrupt with only one-half the cluster mass driven off. The time-scale for impulsive processes must be less than the adiabatic time scale, which is on order of a few crossing times or roughly 3 Myr for ω Cen. If the mass loss is slow enough that the cluster can adjust adiabatically, then the cluster will bloat out such that the cluster radius is inversely proportional to the mass. While this may be the case for a dwarf spheroidal galaxy (which was the goal of the modeling done by Smith), this can hardly be the case for a globular cluster (Gunn 1980).

Smith does point out that if roughly half of the cluster formed stars *before* chemical enrichment happened, then the remaining gas could self-enrich and ultimately be swept out of the cluster by supernovae, without having the cluster disrupt. If this gas fraction leaves slowly enough that the cluster can adjust adiabatically, then the cluster will expand by a modest amount. In support of this latter scenario, he shows that ω Cen has the lowest central concentration for a cluster of its size.

However, at the point where we begin to look into detail about the time scales for mass ejection and star formation, the utility of the Simple Model and its assumption of instantaneous star formation must be questioned. The fact that the free-fall time for a cluster (Fall & Rees 1985), the crossing time, and the typical age for the massive stars are all in the range of $10^6 - 10^7$ yr argues that the chemical enrichment must be tied to the dynamical evolution of the young cluster. One must look towards more dynamical models of cluster formation, which will certainly have

more free parameters. There are many models of cluster formation which try to realistically predict the environment of star formation in a proto-cluster (see, for instance, Fall & Rees 1985, Cayrel 1986, Morgan & Lake 1989, Brown et al. 1991 and 1995, and Vietri & Pesce 1995). As an example, we note the model of Cayrel, as recast by Brown et al. In this model, the proto-cloud center collapses quickly forming a very large OB association. Supernovae and stellar winds from the massive stars produce an annulus of well-mixed enriched material. This annular region forms a second generation of stars which can form a globular cluster if the thermalized stellar velocities are small enough for the stars to be held in the gravitational potential of the cluster. While this model attempts to explain the chemical homogeneity of globular clusters through the turbulent mixing in the annular shell, any explanation for a metallicity spread in ω Cen would be a complication on top of the theory.

We have also detected a weak metallicity gradient in ω Cen. This lends support to an extended time scale for formation of stars, since the metal-rich gas would have time to dissipate its kinetic energy prior to forming stars. However, there is also another interpretation to the metallicity gradient. Previously we noted that the metal-rich stars would be more massive than coeval metal-poor stars. We would then expect the more massive metal-rich stars to sink to the cluster center, on the time scale of the half-mass relaxation time. The relaxation time for the cluster is very large, perhaps half the cluster age, so the effectiveness of the gravitational sinking is hard to estimate without detailed multi-mass King models. Richer et al (1991) do give equilibrium multi-mass models showing a large amount of mass segregation for the most massive stars. The existence of a metallicity gradient outside the half-mass radius where the dynamical time-scales should be much longer than the cluster age would provide strong evidence for dissipative energy loss and an extended time scale for chemical enrichment.

In summary, we find that the functional form of the Simple Model of chemical enrichment gives the same qualitative shape as the metallicity distribution in ω Cen, but in detail, this model underestimates the number of stars on the metal-rich tail. The lack of a resolved metal-poor tail means that ω Cen shares the property with the other Galactic globular clusters that the bulk of the cluster stars formed in a chemically homogeneous environment. Any reasonable fit to the data with the Simple Model requires extremely low yields which in turn implies a cluster mass loss that will bloat the cluster or even more likely cause it to be unbound. The concurrence of important time scales for cluster and stellar formation argue that the Simple Model is inadequate for predicting chemical evolution, and a more dynamical model is required. The metallicity gradient, while supporting the idea of gas dissipation processes leading to a more concentrated later generation of metal-rich stars, also could be an outcome of the sinking of the more massive (but coeval) metal-rich stars over the lifetime of the cluster.

We thank Patrick Seitzer for sharing his list of bright ω Cen giant abundance standards and Pat Côte for a list of NGC 3201 giants. We thank Chris Smith for obtaining CCD observations of ω Cen with the CTIO Schmidt telescope. We acknowledge the help of C. Pryor, H. Richer, P.

Stetson, D. vandenBerg, and G. Wallerstein for discussions on some of the points raised in this work. NBS gratefully acknowledges the hospitality of the Dominion Astrophysical Observatory where much of this paper was written. RPK acknowledges the support from the NSF, under grant AST 92-17970.

A. Appendix

Just as this paper was being completed and prepared for publication, we received a preprint from Norris, Freeman, & Mighell on the metallicity distribution of ω Cen based on 518 giants on the upper RGB ($M_V \gtrsim -1$) using spectra of the Ca II H+K and triplet lines. For 138 stars in common between our BG sample and their sample, we find excellent agreement between the measured Ca II infrared triplet line strengths for all the stars except ROA 320, 336, 383, and 406 where the $W(\text{Ca})$ values differed by more than 0.7\AA . For the remaining 133 stars, a simple linear regression between the two $W(\text{Ca})$ data sets gave a dispersion of 0.15\AA . The Norris et al. study chose to calibrate the data with respect to the $[\text{Ca}/\text{H}]$ values in NDC (see the left-hand panel of Figure 7). A quadratic correlation between the values of $[\text{Fe}/\text{H}]_{NDC}$ in Table 3 as a function of the $[\text{Ca}/\text{H}]$ values given by Norris et al. has a dispersion of only 0.055 dex in $[\text{Fe}/\text{H}]$. Evidently both $W(\text{Ca})$ data sets yield consistent metallicities. The Norris, et al. study finds a secondary hump in the metal rich part of the metallicity distribution which we do not recover in our data. They interpret this second hump as a second generation of stars forming from the enriched ejecta of the primary metal-poor population. While we do not find a secondary hump in our SG sample, we do concur that a simple model for chemical enrichment does not predict the number of metal-rich stars observed.

References

- Alcaino, G. & Liller W. 1984, AJ, 89, 1712
- Armandroff, T.E. 1989, AJ, 97, 375
- Armandroff, T.E., & Da Costa, G.S. 1991, AJ, 101, 1329
- Armandroff, T.E., Da Costa, G.S., & Zinn, R. 1992, AJ, 104, 164
- Bergbusch, P.A., & Vandenberg, D.A. 1992, ApJS, 81, 163
- Bessell, M.S., & Norris, J.E. 1976, ApJ, 208, 369 (erratum 210, 618)
- Binney, J. & Tremaine, S. 1987, in *Galactic Dynamics* (Princeton: Princeton Univ. Press), 514
- Bond, H.E. 1981, ApJ, 248, 606
- Brewer, J. P., Fahlman, G. G., Richer, H. B., Searle, L., & Thompson, I. 1993, AJ, 105, 2158
- Brown, J.H., Burkert, A., Truran, J.W. 1991, ApJ, 376, 115
- Brown, J.H., Burkert, A., Truran, J.W. 1995, ApJ, 440, 666
- Brown, J.A. & Wallerstein, G.W. 1993, AJ, 106, 133
- Butler, D., Dickens, R.J., & Epps, E. 1978, ApJ, 225, 148
- Cannon, R.D. & Stobie R.S. 1973, MN, 162, 207
- Cannon, R.D. 1974, MN, 167, 551
- Carbon, D. F., Langer, G. E., Butler, D., Kraft, R. P., Suntzeff, N. B. Kemper, E., Trefzger, C. F., Romanishin, W., 1982, ApJS, 49 207
- Cayrel, R. 1986, A&A, 168. 18
- Chun, M.S., & Freeman, K.C. 1978, AJ, 83, 376
- Cohen, J.G. 1981, ApJ, 247, 869
- Côte, P., Welch, D. L., Fischer, P., Da Costa, G. S., Tamblyn, P. Seitzer, P., & Irwin, M. J. 1994, ApJS, 90, 83
- Cudworth, K.M., & Rees, R. 1990, AJ, 99, 1491
- Cudworth, K.M. 1994, private communication
- Da Costa, G.S., Armandroff, T.E., & Norris, J.E. 1992, AJ, 104, 154
- Da Costa, G.S. & Villumsen, J.E. 1981, in *Astrophysical Parameters for Globular Clusters*, eds A.G.D. Philip & D.S. Hayes, (Schenectady; Davis) 527
- Dickens, R.J., Feast, M.W., & Lloyd Evans T. 1972, MNRAS, 159, 337
- Dickens, R.J., & Saunders, J. 1965, Roy. Obs. Bull., No. 101
- Eggen, O.J. 1972, ApJ, 172, 639
- Erdelyi-Mendes, M. & Barbuy, B. 1991, A&A, 241, 176
- Fall, S.M. & Rees, M.J. 1985, ApJ298, 18
- Freeman, K.C. 1985, in IAU Symp. 113, p. 33
- Francois, P, Spite, M., & Spite, F. 1987, A&A, 191, 267
- Fusi Pecci, F., Ferraro, F. R., Crocker, D. A., Rood, R. T., & Buonanno, R. 1990, A&A, 238, 95
- Gingold, R.A. 1974, ApJ, 193, 177

- Gratton, R.G. 1982, *A&A*, 115, 336
- Gunn, J.E. 1980, in *Globular Clusters*, eds D. Hanes & B. Madore (Cambridge: Cambridge) 301
- Hartwick, F.D.A. 1976, *ApJ*, 209, 418
- Hartwick, F.D.A. 1983, *Mem. S.A. It.*, 54, 51
- Hawarden, T.G. & Epps Bingham, E.A. 1987, *SAAO Circ*, 11, 83
- Hesser, J.E. Hartwick, F.D.A., & McClure, R.D. 1977, *ApJS*, 33, 471
- Kraft, R.P. 1994, *PASP*, 106, 553
- Langer, G.E., Suntzeff, N.B., & Kraft, R.P. 1992, *PASP*, 104, 523
- Lee, S.-W. 1977a, *A&AS*, 27, 367
- Lee, S.-W. 1977b, *A&AS*, 27, 381
- Lee, S.-W. 1977c, *A&AS*, 28, 409
- Lloyd Evans, T. 1974, *MNRAS*, 167, 393
- Lloyd Evans, T. 1983a, *SAAO Circ*. 7, 86
- Lloyd Evans, T. 1983b, *MNRAS*, 204, 975
- Mallia, E.A., & Pagel, B.E.J. 1981, *MNRAS*, 194, 421
- Martin, W.L. 1981, *SAAO Circ*, 6, 28
- Matteucci, F. 1983, *Mem. S.A. It.*, 54, 289
- Mayor, M., Imbert, M., Andersen, J., Ardeberg, A., Baranne, A., Benz, W., Ischi, E., Lindgren, H., Martin, N., Maurice, E., Nordström, B., & Prévot, L. 1983, *A&AS*, 54, 495
- Meylan, G. & Mayor, M. 1986, *A&A*, 166, 122
- Morgan, S., & Lake, G. 1989, *ApJ*, 339, 171
- Nemec, J.M., & Harris, H.H. 1987, *ApJ*, 316, 172
- Norris, J. 1980, in *Globular Clusters*, eds. D. Hanes & B. Madore (Cambridge: Cambridge), 113
- Norris, J. & Smith, G.H. 1983, *ApJ*, 272, 635
- Norris, J. & Bessell, M.S. 1975, *ApJ*, 201, L75 (erratum in 210, 618)
- Norris, J. & Bessell, M.S. 1977, *ApJ*, 211, L91
- Norris, J.E., & Da Costa, G.S. 1995, *ApJ*, 447, 680
- Olszewski, E. W., Schommer, R. A., Suntzeff, N. B., & Harris, H. C. 1991, *AJ*, 101, 515
- Pagal, B.E.J. 1992, in *The Stellar Populations of Galaxies*, IAU Symp. 149, eds. B. Barbuy & A. Renzini (Dordrecht: Kluwer) 133
- Paltoglou, G. & Norris, J.E. 1989, *ApJ*, 336, 185
- Persson, S. E., Cohen, J. G., Matthews, K., Frogel, J. A., & Aaronson, M. 1980, *ApJ*, 235, 452
- Peterson, R. C., Rees, R. F., Cudworth, K. M. 1995 *ApJ*, 443, 124
- Press, W.H., Teukolsky, S.A., Vetterling, W.T., & Flannery, B.P. 1992, *Numerical Recipes*, (Cambridge: Cambridge, MA), p. 617

- Pryor, C. & Meylan, G. 1993, in *Structure and Dynamics of Globular Clusters*, ASP Conf. Series Vol 50, eds. S.G. Djorgovski & G. Meylan (San Francisco: ASP) 357
- Richer, H.B., Fahlman, G.G., Buonanno, R., Fusi Pecci, F., Searle, L., & Thompson, I.B. 1991, *ApJ*, 381, 147
- Sandage, A.R., & Cacciari, C. 1990, *ApJ*, 350, 645
- Searle, L., & Sargent, W.L.W. 1972, *ApJ*, 173, 25
- Smith, G.E. 1984, *AJ*, 89, 801
- Stetson, P.B. 1994, *PASP*, 106, 250
- Suntzeff, N.B. 1981, *ApJS*, 47, 1
- Suntzeff, N.B. 1993, in the *Globular Cluster-Galaxy Connection*, ASP Conf. Series, Vol 48, eds G.H. Smith & J.P. Brodie (San Francisco: ASP) 167
- Suntzeff, N.B., Kraft, R.P., & Kinman, T.D. 1994, *ApJS*, 93, 271
- Suntzeff, N. B., Schommer, R. A., Olszewski, E. W., & Walker, A. R. 1992, *AJ*, 104, 1743
- Suntzeff, N.B., Mateo, M., Terndrup, D.M., Olszewski, E.W., Geisler, D., & Weller, W. 1993, *ApJ*, 418, 208 (S93)
- Trager, S.C., King, I.R., & Djorgovski, S. 1995, *AJ*, 109, 218
- Vandenberg, D.A. 1991, *ApJ*, 391, 685
- Vietri, M. & Pesce, E. 1995, *ApJ*, 442, 618
- Webbink, R.F. 1985, in *IAU Symp. 113, Dynamics of Star Clusters*, ed. J. Goodman & P. Hut (Dordrecht: Reidel) 541
- Willey, R. 1961, *ApJ*, 133, 430
- Woolley, R. v.d.R. 1966. *Royal Obs. Ann.*, No. 2
- Woolley, R.v.d.R., Alexander, J.B., Mather, L., & Epps, E. 1961, *Roy. Obs. Bull. No.* 43
- Zinn, R. 1978, *ApJ*, 225, 790
- Zinn, R., & West, M.J. 1984, *ApJS*, 55, 45

Figure Captions

Fig. 1.— A color-magnitude diagram showing the two sample regions in ω Cen observed in this study. The BV photometry is from Woolley (1966). Only stars with small proper motions are plotted.

Fig. 2.— A color-magnitude diagram of ω Cen showing the stars observed in this study. The filled circles represent radial velocity members and the exes non-members. The BV photometry is from Woolley (1966).

Fig. 3.— The error in a single observation plotted as a function of the logarithm of the mean intensity in the co-added spectrum. The upper plot presents the data for the $W(\text{Ca})$ errors in units of (\AA), and the lower plots presents the velocity errors in units of km s^{-1} . The curves represent the median points in the distributions.

Fig. 4.— The Ca II infrared triplet equivalent width $W(\text{Ca})$ in units of (\AA) plotted as a function of the V magnitude with respect to the cluster horizontal branch for giants in the calibrating clusters.

Fig. 5.— The Ca II infrared triplet equivalent width $W(\text{Ca})$ in units of (\AA) for the bright and faint star sample plotted as a function of $(V - V_{HB})$.

Fig. 6.— The cluster $[\text{Fe}/\text{H}]$ from Zinn & West (1984) plotted as a function of the averaged “reduced” equivalent widths in units of (\AA) for the calibrating clusters (1984). The closed circles are data from this work (NGC 3201) or S93, and the open circles are from Armandroff et al. (1992) and Armandroff & Da Costa (1991). The solid lines are the best fits providing a continuous relationship which were used to calculate $[\text{Fe}/\text{H}]_{ZW}$ for the ω Cen giants.

Fig. 7.— A comparison of the reduced equivalent width W' in units of (\AA) with the calcium and iron abundances in individual stars in ω Cen. The detailed abundances were taken from Norris & Da Costa (1995). The dotted line is the relationship given in the text to calculate $[\text{Fe}/\text{H}]_{NDC}$. The open circles are some other globular cluster stars observed by Norris & Da Costa (1995) for which we also have W' values.

Fig. 8.— Spectra of the Ca II infrared triplet region for the SG sample ω Cen giants showing the range in line strength. From top to bottom the stars are ROA 1317 ($[\text{Fe}/\text{H}]_{NDC} = -1.81$), ROA 5612 (-1.30), and ROA5017 (-1.04). All the spectra have been normalized to a continuum value of 1 and shifted by increments of 0.5.

Fig. 9.— Dereddened $(B - V)_0$ values plotted as a function of $[\text{Fe}/\text{H}]$ for the SG sample. The data are plotted on the ZW scale (left panel) and the NDC scale (right panel). The relationship for $(B - V)_{0,g}$ as a function of $[\text{Fe}/\text{H}]$ from Webbink (1985) is shown as the solid line. The range

in metallicity is better fit by the NDC scale.

Fig. 10.— The multiplicative correction factor to correct the observed number of stars binned as a function of metallicity in the SG or BG sample to an equivalent number of main sequence stars just below the turn off. The solid line is the correction for the SG sample and the dotted line is the correction for the BG sample. These correction factors were calculated for a mass function exponent of $x = 1$.

Fig. 11.— The metallicity histograms for the cluster ω Cen. These histograms have been corrected for evolutionary effects, and represent the relative number of stars between 0.6 and $0.7M_{\odot}$ as a function of metallicity. The solid-line histogram represents the SG sample and the dotted-line histogram the BG sample. The left panel is on the Zinn & West (1984) metallicity scale, and the right panel is on the Norris & Da Costa (1995) scale. The BG sample has been scaled to the sample size of the SG sample to allow comparison.

Fig. 12.— Plot of radial gradient (in units of arcminutes) of metallicity in ω Cen. The left panel shows the BG sample (solid circles) and the Seitzer bright giants (open circles). The right panel shows the SG sample. The metallicities are plotted on the NDC scale.

Fig. 13.— Histogram of the metallicity distribution for the SG sample compared to an example fit to a simple model of chemical evolution. The solid curve is the histogram of observed $[\text{Fe}/\text{H}]$ values on the $[\text{Fe}/\text{H}]_{NDC}$ scale. The dotted line curve is the model (on an arbitrary vertical scale), and the solid line curve is the model convolved with a gaussian of dispersion of 0.07 dex in $[\text{Fe}/\text{H}]$. The dotted histogram is the histogram of the convolved model scaled to the observed data.

TABLE 1. Globular Clusters Used for Calibration

TABLE 2. Photometry, EQW values, and Radial Velocities for Standard Clusters

TABLE 3a. Photometry, EQW values, and Radial Velocities for ω Cen BG Sample

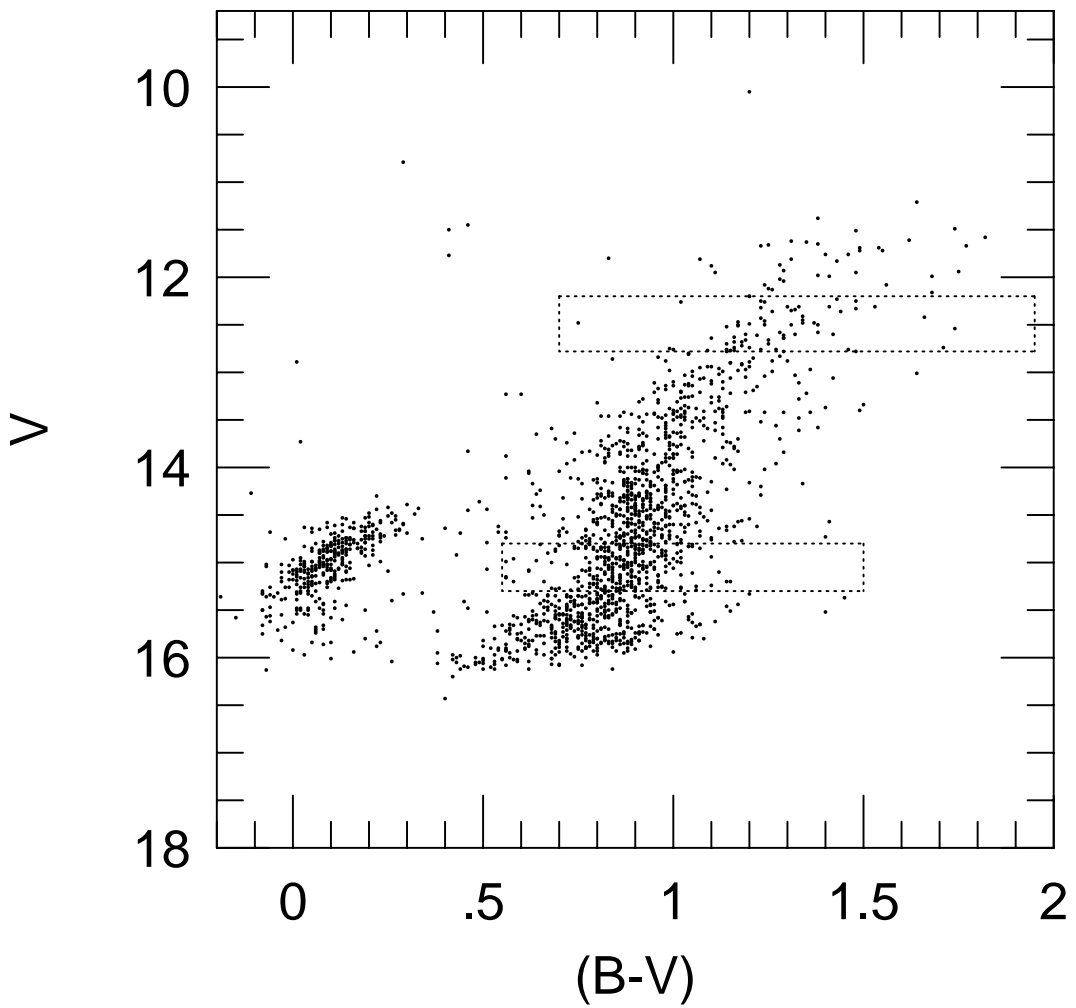
TABLE 3b. Photometry, EQW values, and Radial Velocities for ω Cen SG Sample

TABLE 4. ω Cen Velocity Non-Members

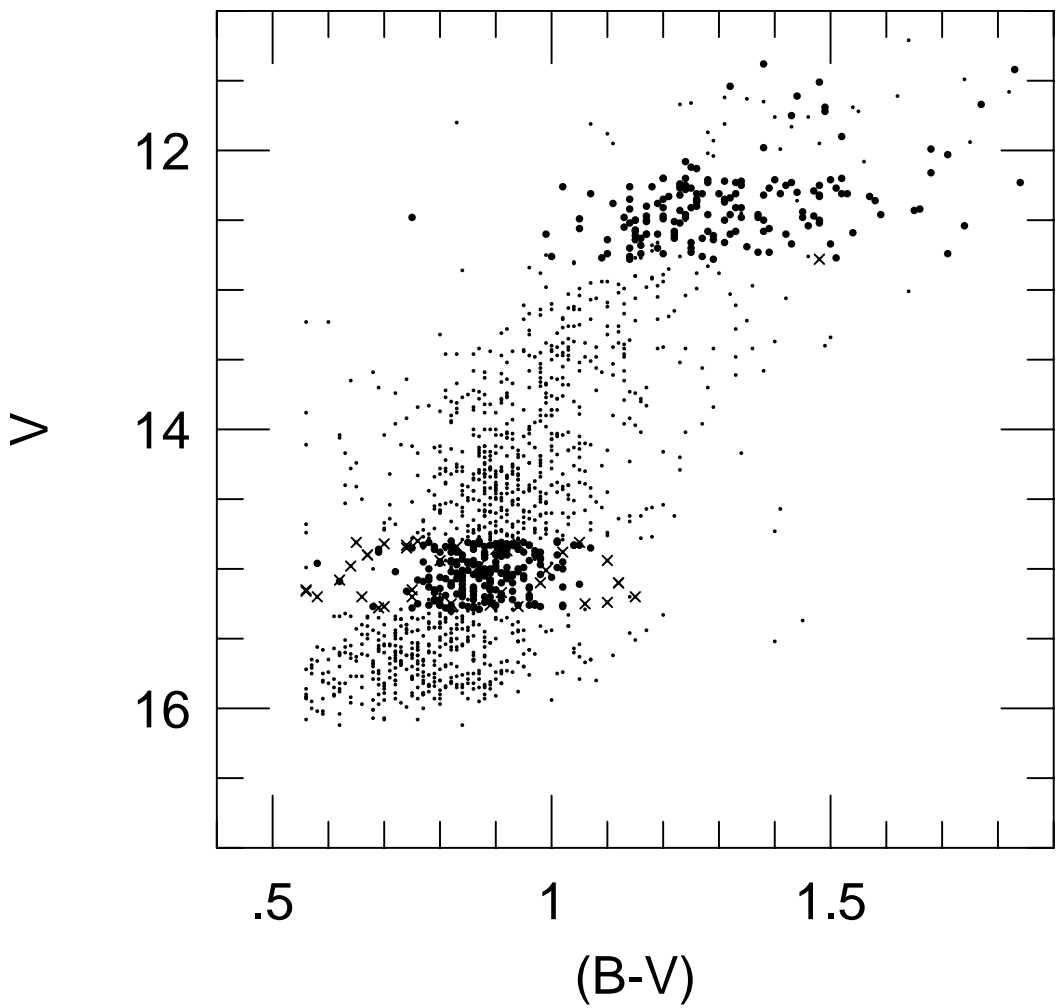
TABLE 5. Velocity Comparisons

TABLE 6. Median Values for the Error in a Single Observation

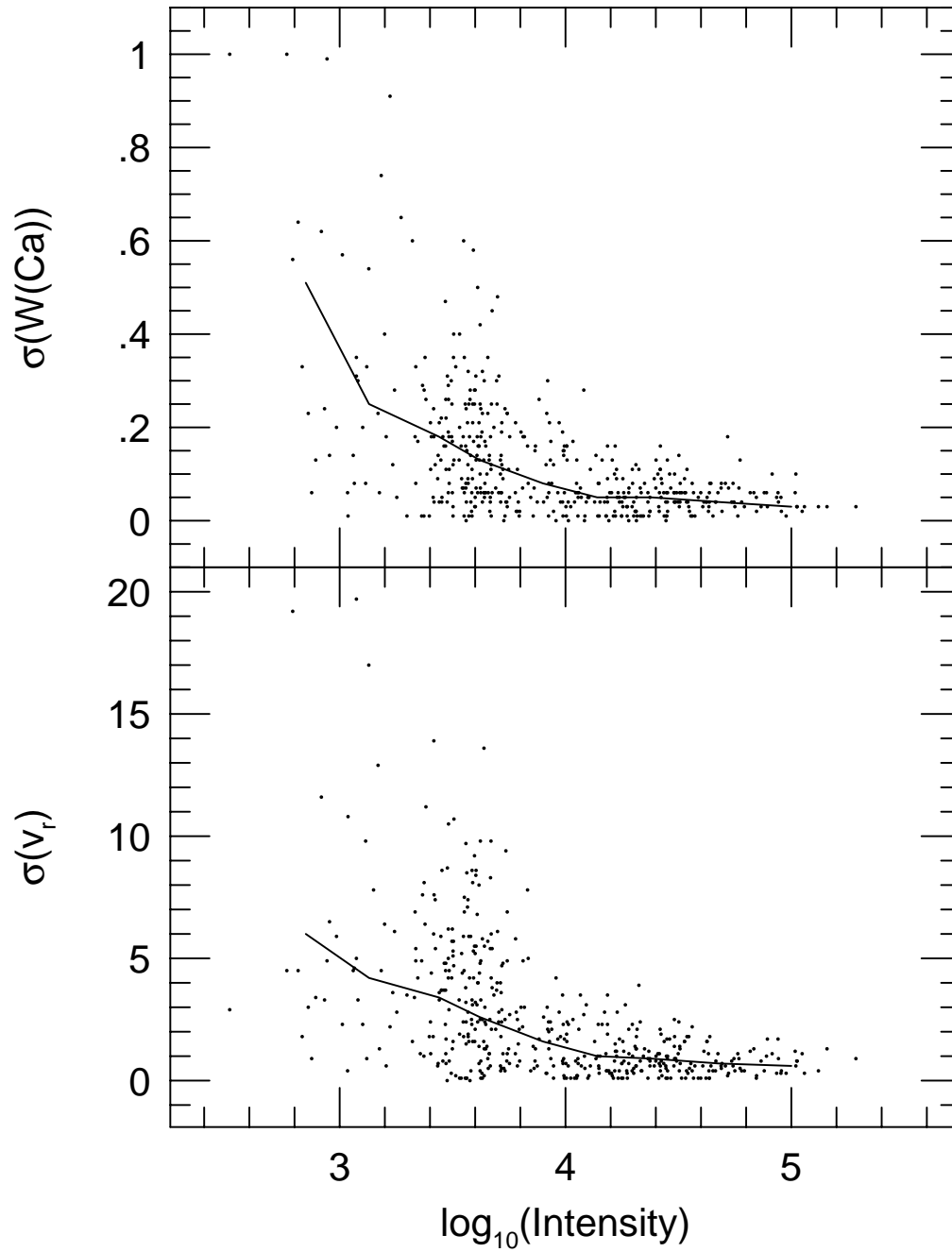
TABLE 7. Metallicity Averages for ω Cen



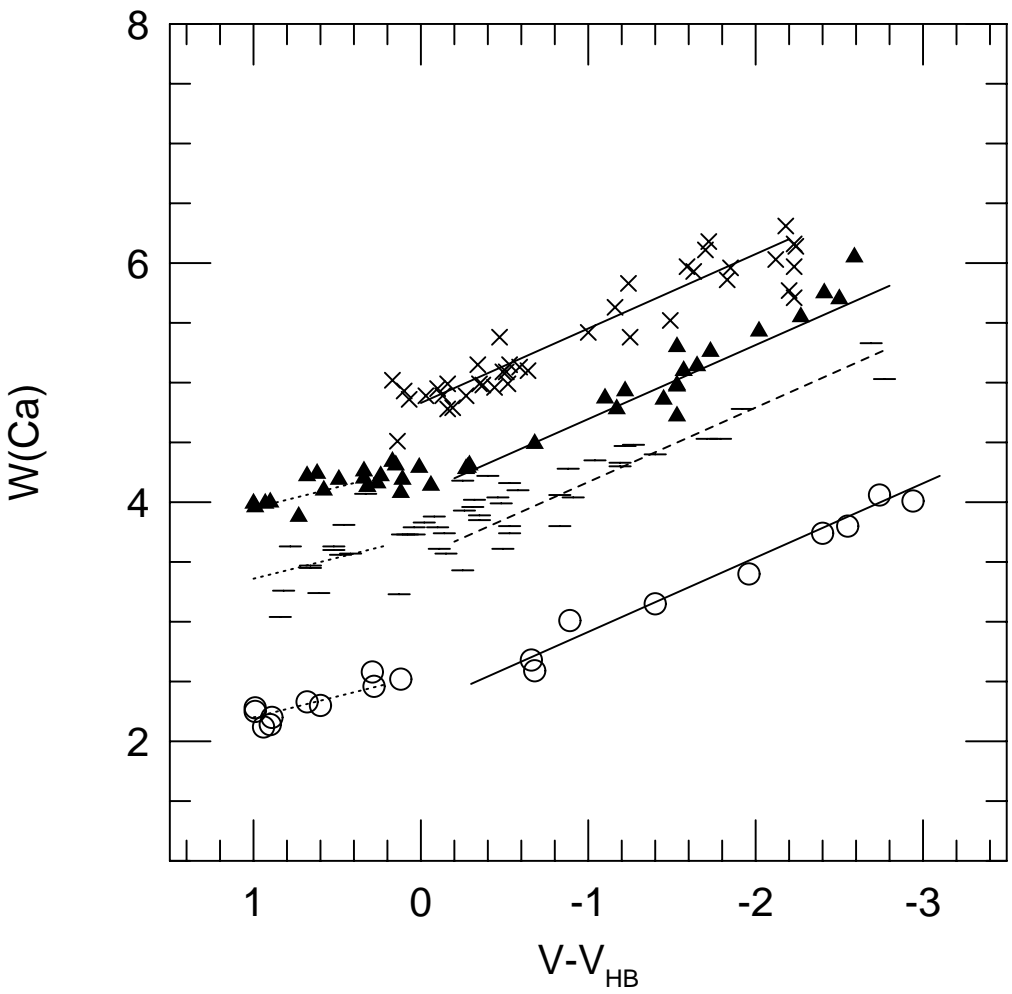
Suntzeff and Kraft, Figure 1



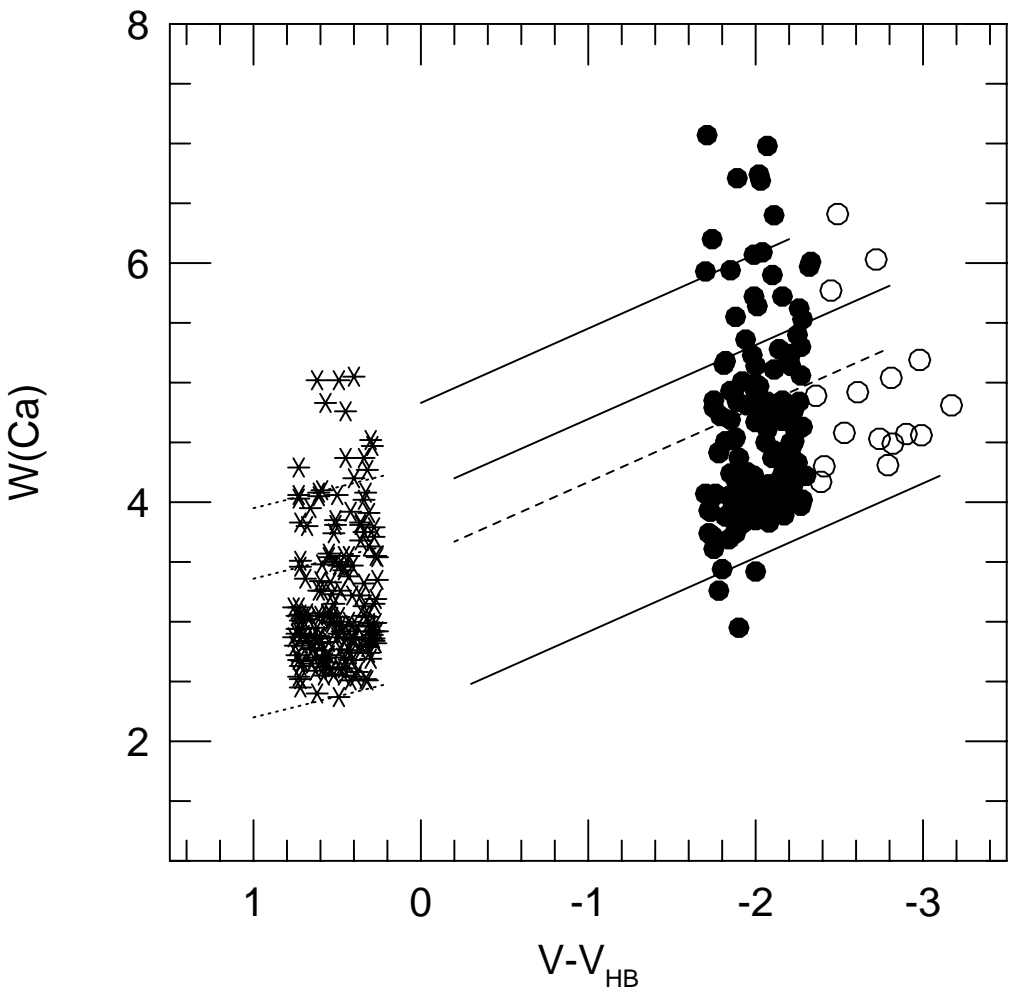
Suntzeff and Kraft. Figure 2



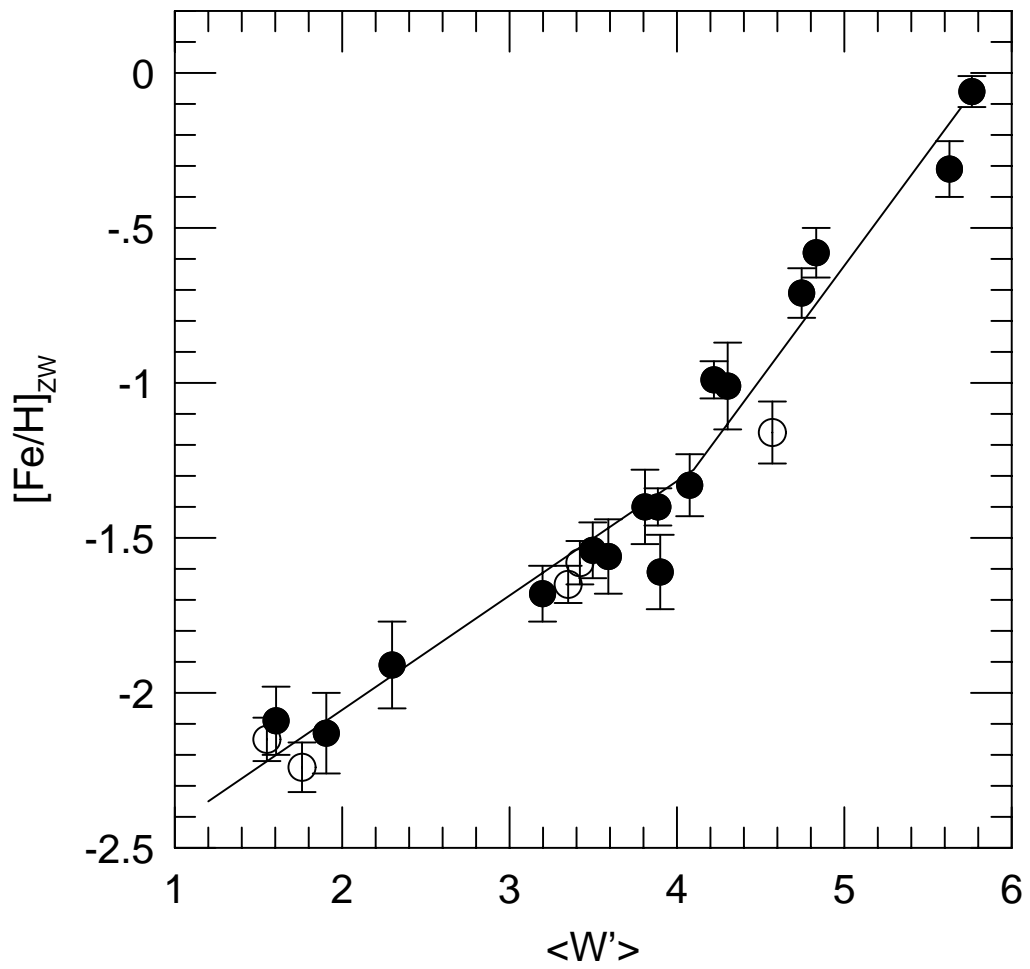
Suntzeff and Kraft. Figure 3



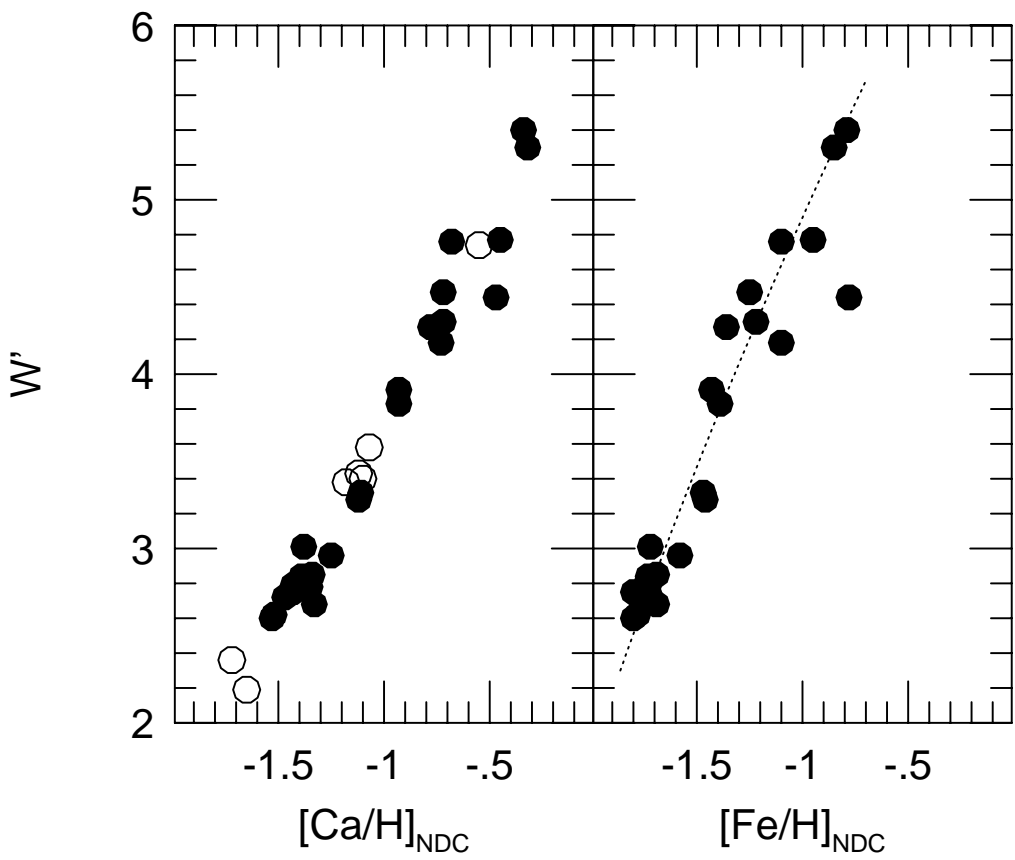
Suntzeff and Kraft, Figure 4



Suntzeff and Kraft, Figure 5

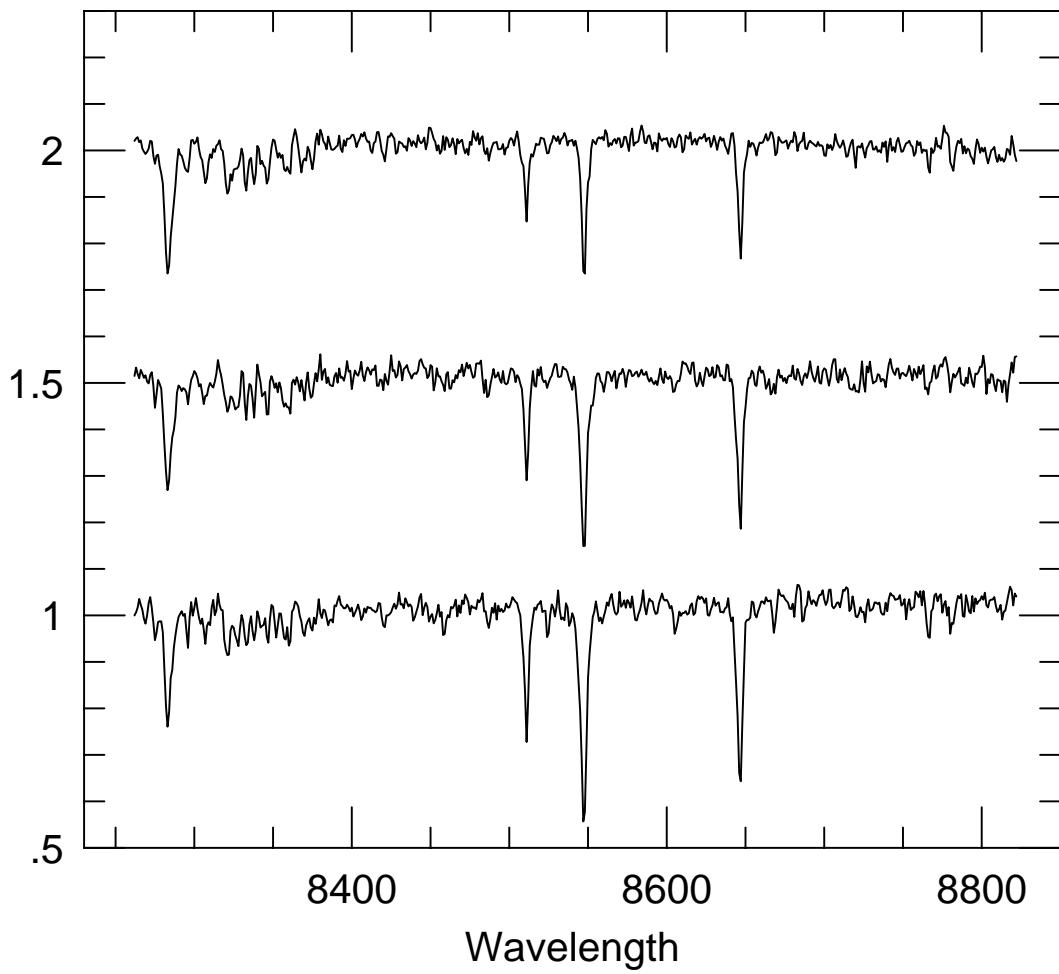


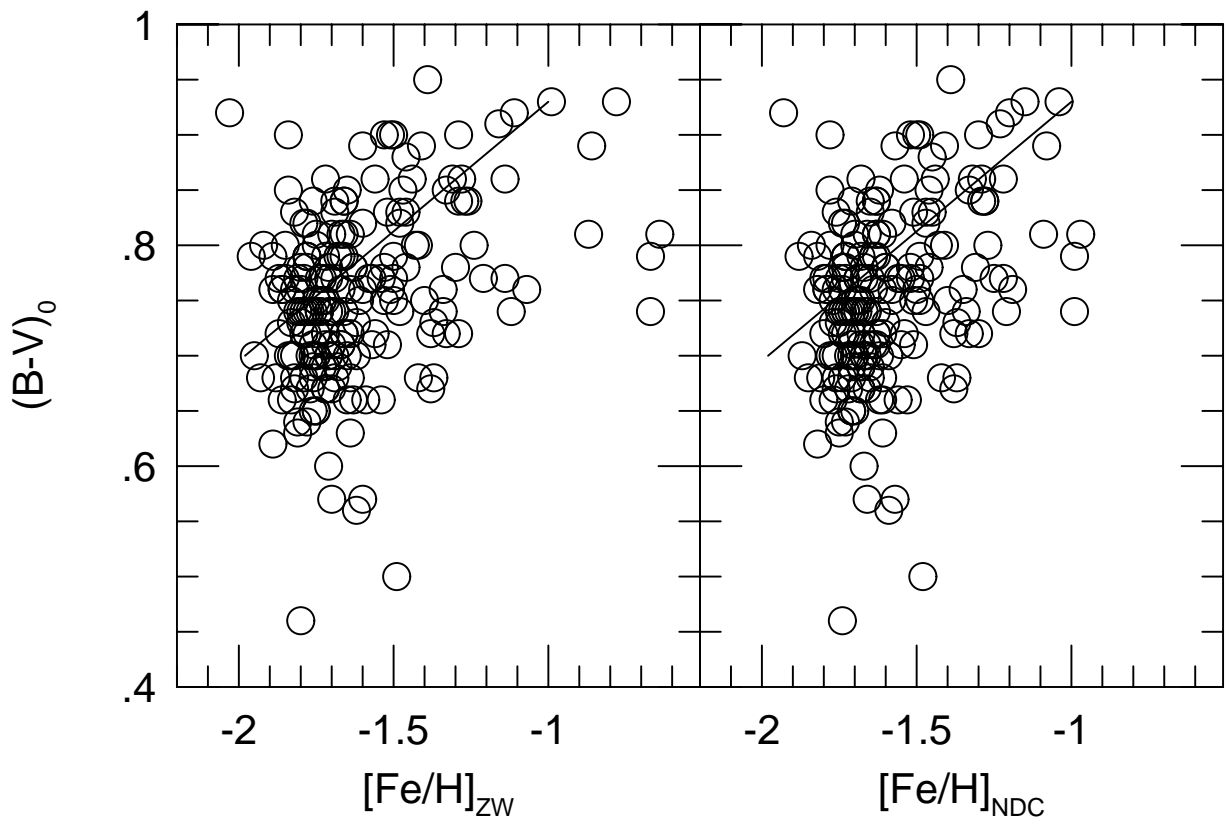
Suntzeff and Kraft. Figure 6



Suntzeff and Kraft. Figure 7

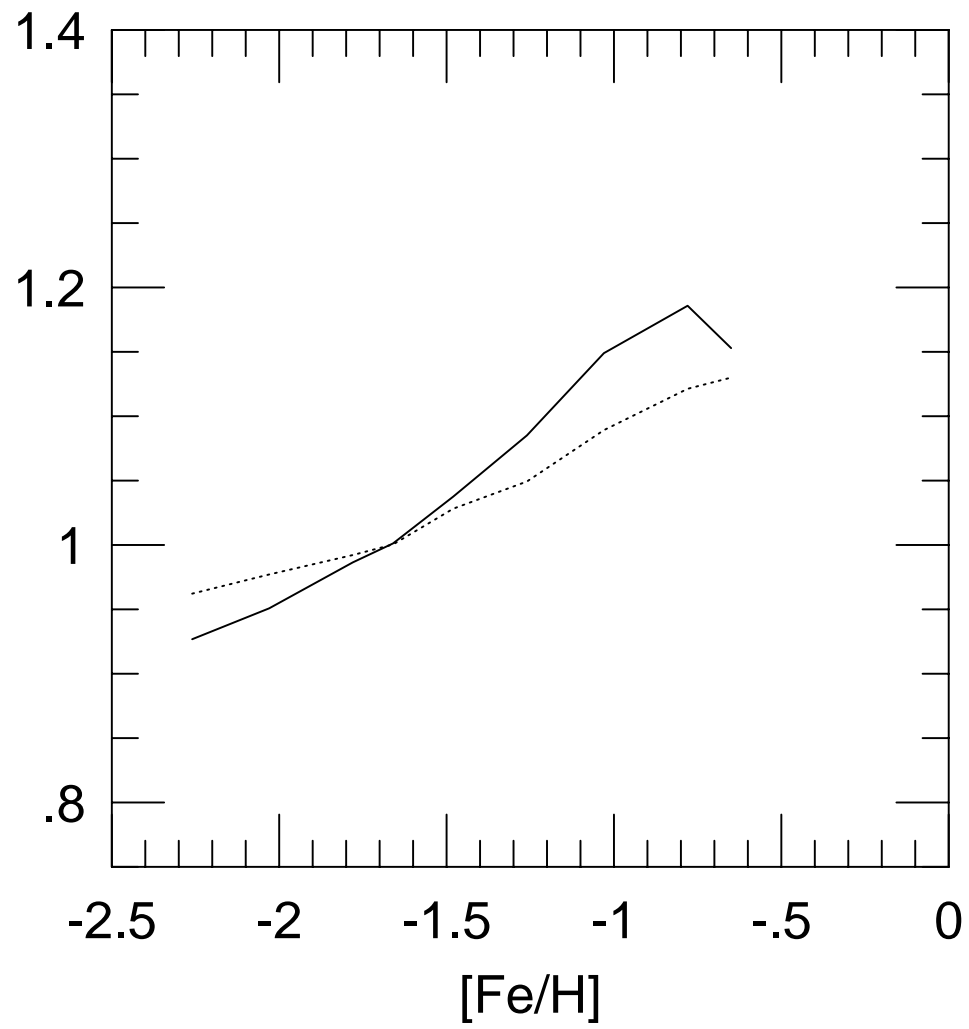
Suntzeff and Kraft, Figure 8



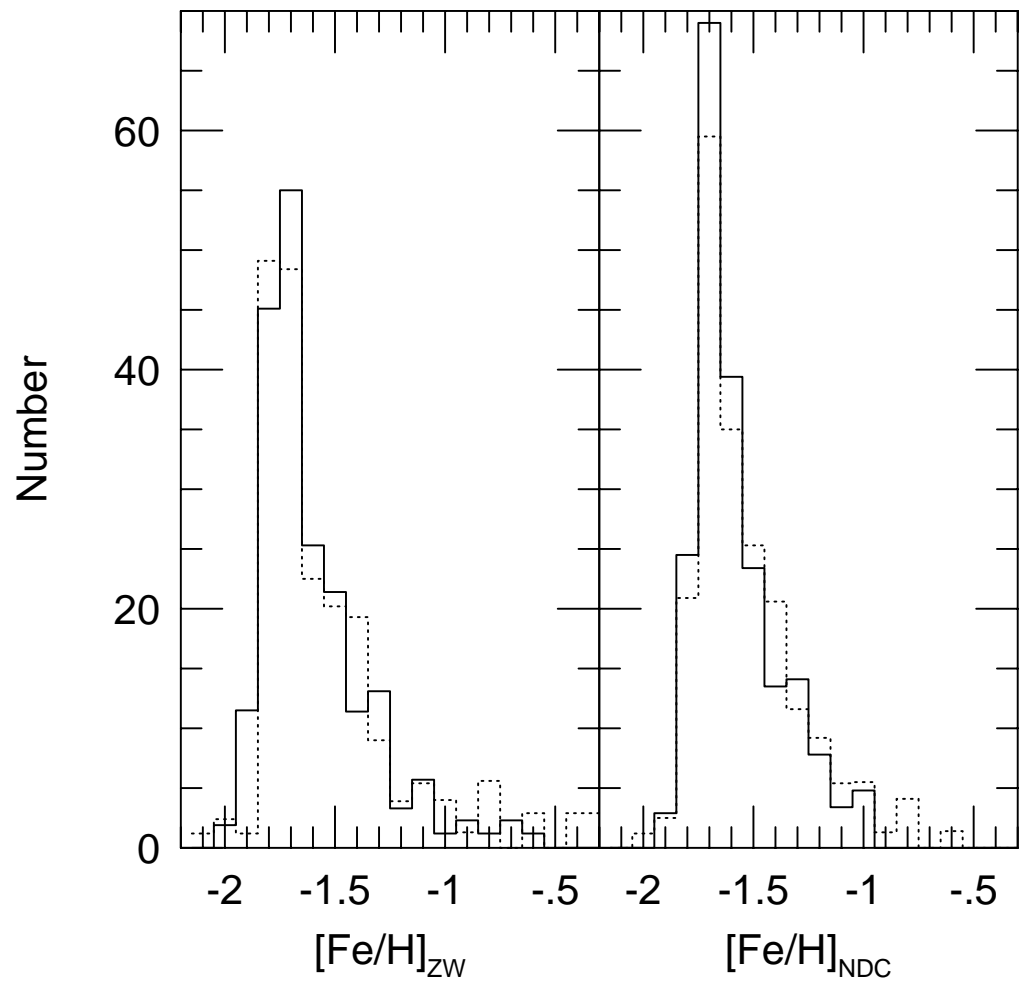


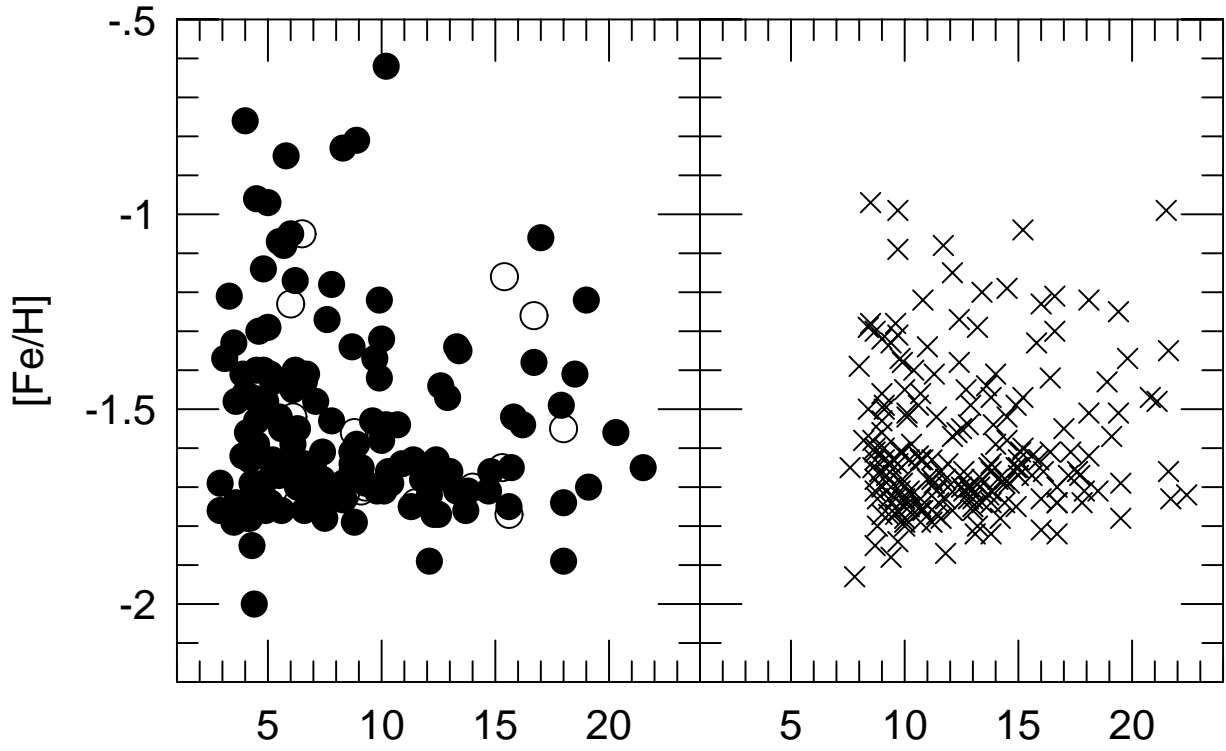
Suntzeff and Kraft, Figure 9

Suntzeff and Kraft. Figure 10

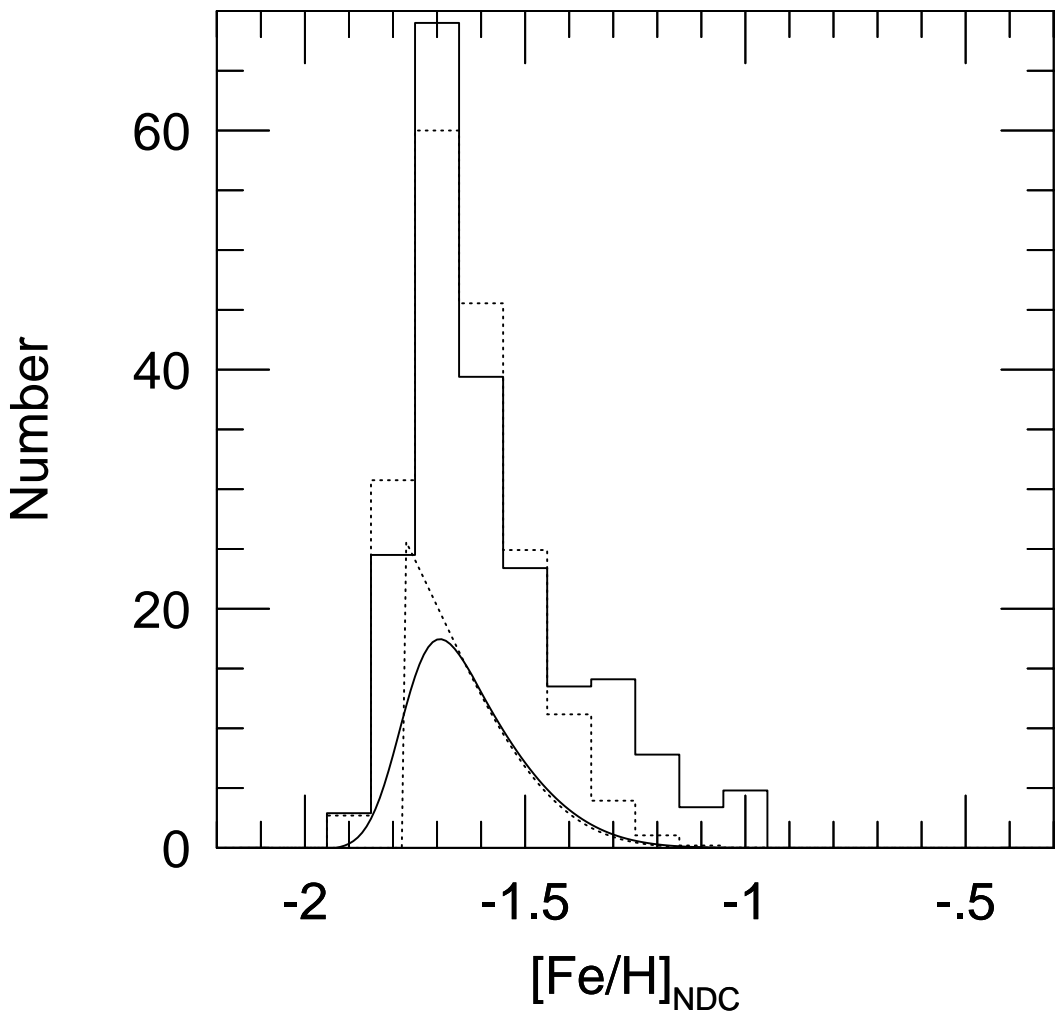


Suntzeff and Kraft. Figure 11





Suntzeff and Kraft. Figure 12



Suntzeff and Kraft. Figure 13